SECOND APPLICATION OF THE "SUCCESSIVE TRANSFORMATIONS METHOD" TO PREDICT THE SAFEST LUNAR LANDING SITE FOR AN ASTRONAUT REPORT 3

By

Hector R. Rojas, Ph. D.

Prepared by:

Lockheed Electronics Company
Houston Aerospace Systems Division
Houston, Texas

For

National Aeronautics and Space Administration
Manned Spacecraft Center
Houston, Texas

July 1967

70058

TABLE OF CONTENTS

SECOND APPLICATION OF THE "SUCCESSIVE TRANSFORMATIONS METHOD" TO PREDICT THE SAFEST LUNAR LANDING SITE FOR AN ASTRONAUT

REPORT 3

By Hector R. Rojas, Ph. D.

INTRODUCTION

The purpose of the first application of the "Successive Transformations Method" described in the second report was to determine, for a manned spacecraft, the optimum landing site on the moon. The results obtained, made by extrapolating the temperature T_0 furnished by Surveyor, can be summarized as follows: (1) The method is efficient in allowing selection of the optimum landing area. (2) The area selected is extensive and relatively flat; consequently, it is sufficient to allow trine for the difficult landing operation which results from the high speed of the spacecraft when reaching the moon. (3) The relative temperature obtained is lower than that where Surveyor landed.

In this third report, a second application of the "Successive Transformations" is described to determine the safest conditions of a given landing site for the astronaut, especially in relation to determining the composition of the lunar surface material. As a means of accomplishing this task, it is the intent of this paper to analyze lunar craters since they are present over so much of the lunar surface.

The conclusions reached in the second report, as well as those in the third report, are the basis for analyzing Orbiter photographs; consequently, we are obligated to discuss first some problems regarding stereographic measurements and their interpretation. The reason for this is to allow comparison of the albedos determined in this report with those given by the standard lunar photometric contours to see how well the values match when analyzing the Orbiter photographs. In discussing image quality, we need to be sure that photographs of landing sites have good contrast so that they can be related with different albedos of the lunar area under examination.

For example, we know that there are many cases in lunar photography in which high quality images are recorded for an area or for an entire hemisphere but the coverage is monoscopic. This is generally true for earth-based astronomical observations where the synchronous rates of lunar revolution and rotation caused the same hemisphere to be turned toward the observer. The variation of the direction of perspective due to the lunar librations is not adequate to permit stereographic measurements of local variations in the topography of the moon. The Orbiter's low resolution photographic coverage has provided good stereographic coverage from which topographic measurements can be made. Their high resolution photographs sometimes have very little overlap, but this is due to the photographic mode selected.

The method based on measurement and reduction of shadow lengths has long been used as a means for obtaining relative heights of objects, both in photogrammetry and in lunar

astronomy. However, there are limitations in the application of this procedure since it requires that the slope gradients exceed the angle of illumination. When observations are made at the low sun angles required to obtain the sensitivity required in using the shadow method, there is a general masking of detail in the area because of the number and size of the shadows cast. The alternative approach to this problem has been the analysis of the photometric output of the lunar surface under any given combination of observation and illumination angles, with the objective of interpreting photometric differences across an area resulting from change of local slope. These slopes can be integrated along the direction of illumination to yield relative height information.

For the analysis of the Orbiter's photographic images, which will be examined in more detail in a succeeding report, it will be necessary to do a rigorous evaluation of the intensity transfer function of the camera lens and sensor system to describe the field pattern that the camera imposes upon the observed scene brightness. Present interpretation of lunar topography utilizes the application of photometry to topography through the observer's advance knowledge of what the brightness output of the landing site surface should be. If variation of brightness is found in the photograph of a given landing site, then the observer must have at hand the photometric properties of the surface material under study to permit identification of the sources of variation and to interpret the information quantitatively.

From all that has been described, one can see how important it is to make a joint analysis of the Orbiter's photographs by considering the following aspects: (1) Establish

height evaluation differences between images taken from 28 and 238,900 miles, respectively (from Orbiter and from earth). (2) Apply the photometry to topographic studies of the landing sites to establish analysis of the eventual brightness variation. (3) Use the slope, η/N, from the Surveyor study, second report, to help discriminate in the same manner between the height evaluation differences mentioned above. The albedos obtained from this report will help in the analysis of brightness variation described above. By utilizing all these data in conjunction with the study of Orbiter photographs, we shall be in a better position to obtain qualitative information about any of the landing sites proposed by NASA so that a final choice can be made. This is what we intend to do at a later time.

Chapter 1

DEFINITION OF THE METHOD FOR ALBEDOS

The application of the method of "Successive Transformations" for determining albedos requires a review of previous reports describing the method. From Scheme 4, shown on page A-4 of the first report, we shall utilize the slope, η/N, to analyze the variation of albedos in any lunar area from its border to its center. In a similar manner, as pointed out in page 9 of the second report, we shall use the differences found in the effective temperature increments, δT_0, to establish relatively flat surfaces, elevations, craters and depressions. In other words, instead of making unnecessary computations, we shall use the values of δT_0 obtained from Surveyor's data and the corresponding values of η/N to establish the variation in albedo. To aid in understanding this method, consider that there would not be an albedo variation on the moon if only flat, smooth surfaces of homogenous composition existed. Since this is not the case, we have the following four variations:

$$\left(\delta T_0/\frac{\eta}{N}\right) \cdot t = A_1 \text{ for relatively flat surface}$$

$$\left(\delta T_0/\frac{\eta}{N}\right) \cdot x = A_2 \text{ for elevations}$$

$$\left(\delta T_0/\frac{\eta}{N}\right) \cdot y = A_3 \text{ for craters}$$

$$\left(\delta T_0/\frac{\eta}{N}\right) \cdot z = A_4 \text{ for depressions ,}$$

where A_1, A_2, A_3 and A_4 represent the corresponding albedos of the different topographic characteristics t, x, y

and z mentioned above. However, in the case of the moon, topographic relief is not continuous. That is, a given relatively flat surface is interrupted by craters, depressions or small elevations. The same thing can be said for mountainous formations and large craters. As a consequence, the characteristics t, x, y and z of such topographic relief are much more complex to define.

Procedure for Obtaining Albedos

To obtain the correct albedos from the values of (η/N) and δT_0, proceed in the following manner:

1. Select the points of interest on the lunar map for each type of topographic relief considered.
2. Superimpose on that lunar map the transparent overlay of effective temperature contours mentioned in the second report.
3. For each lunar relief feature considered, read the T_0' from the North to the South and from the West to the East through the center of the area where readings of such T_0' are made. (The center of the area is the center of the lunar relief feature.) Next, take the difference values of δT_0 between North → South and East → West readings; let us write such differences as $\widehat{\delta T_0}$ to note that they belong to either a central point of a relatively flat surface, to the vertex of a crater, or to the top of an elevation.
4. When reading the value of T_0' on the transparent overlay superimposed on the lunar map, make note of the values η and N to compute the slopes (η/N).

5. With the values (η/N) and $\widehat{\delta T_0}$ for each lunar feature, compute their corresponding albedos using the equations that follow. These albedos will be designated A_0 to indicate that they are obtained from T_0 furnished by Surveyor. Since by definition the expression $\delta T_0/\frac{\eta}{N}$ corresponds to the absorption of sunlight by the lunar surface, the A_0 is an "equivalent albedo" as compared with the albedo which is measured on earth. In other words, the "equivalent albedo A_0" is the remaining sunlight which is reflected after a fraction of such sunlight is absorbed by the lunar surface. The albedo measured on earth, therefore, corresponds to reflected sunlight.

Definition of "Equivalent Albedo A_0" and the Earth Albedo

To better understand the respective definitions of the "equivalent albedo A_0" and the albedo measured on earth, let us examine Scheme VI of this report and point out the following facts: (1) A fraction of the sunlight is absorbed by the lunar material. (2) Another fraction is scattered by the surface itself and the importance of such scattered sunlight depends on the grainsize and the topographic irregularities of the lunar surface. (A more detailed treatment of the scattering of sunlight will be presented in the next report.) (3) Finally, the remaining sunlight is reflected.

On the other hand, the reflected sunlight from the moon encounters the following modifications: (1) A fraction of the reflected sunlight is scattered by our atmosphere. (2) The direction of the reflected beam is modified by the air mass.

(3) The said reflected sunlight suffers more important atmospheric absorption in certain wavelengths than in others; in other words, the earth's atmospheric absorption is not homogenous.

Obtaining "Equivalent Albedo A" from the T_0 Furnished by Surveyor

Since the moon does not have an atmosphere, sunlight penetrates into the lunar surface to a depth that depends on the wavelength. This has been indicated in the graph of Scheme VI. The depth reached by a given wavelength of light depends on the nature of the lunar material. From the practical point of view when making earth-based observations, the lunar surface composition of a given area can be studied by taking the color indices (U - B) , (B - V) , etc. But in view of the fact that earth atmospheric absorption varies with the wavelength, it is better to observe this phenomenon at high altitudes (more than 10,000 feet) in order to get data of good quality.

Besides the penetration of the sunlight into the surface, Scheme VI shows that infrared energy also is radiated from the moon. So the radiation that we receive from the moon is composed of reflected sunlight and thermal radiation produced by the moon itself. The lunar thermal radiation is independent of the nature of its surface materials and depends only on the temperature of these materials. For this reason, if any useful information is to be obtained from Surveyor, it should be in the spectral regions where the thermal radiation effects are negligible. Under sunlit conditions, the intensity of the

sunlight equals the intensity of the thermal radiation in the wavelength region of 3 microns. For wavelengths shorter than this, the sunlight is dominant, but the opposite happens in the case of longer wavelengths and infrared radiation prevails.

Therefore, between observations from Surveyor on the moon and those made from earth, we have the following two differences: (1) The wavelength region of 3 microns is important for the "equivalent albedo A_0" from the T_0 furnished by Surveyor. (2) The wavelength region of earth-based observations is smaller by 0.5 microns than that already mentioned; this is due to atmosphere opacity. From (1) and (2), we see that photometric observations with an accuracy of a few percent will limit the long wavelength end of a spectral survey to the 2-microns region if lunar surface temperatures enable corrections such that meaningful data can be extended to about 2.5 microns. Beyond this, the earth's atmosphere is opaque to about 3.4 microns and the lunar radiation is dominant. As a consequence, it appears that the practical long wavelength for earth-based observations is about 2.5 microns.

From this discussion, we see now why T_1 and T_2 of Scheme VI are equal. We deal only with an infinitely thin layer of the lunar surface since this is the case of the near infrared end of $\lambda = 3\mu$. In the same manner, we see also that the T_0 of Surveyor corresponds to infinitely thin layers of the lunar surface. Because of this, and since the case mentioned remains free of the sunlight penetration into the lunar surface that results from the variation of wavelength, we can finally write as follows:

$$\left[100\left(\widehat{\delta T}_0/\frac{\eta}{N}\right)\right] \cdot A_0 = \frac{T_0}{T_1} ,$$

but, since $T_0/T_1 = 1$ for $\lambda = 3\mu$,

$$\text{then (14)} \quad A_0 = \left(100 \frac{N}{\eta} \widehat{\delta T}_0\right)^{-1}$$

With the application of equation (14) to the different lunar reliefs of interest, we can compare its exponential curve with the standard lunar photometric contour previously mentioned. We shall do this for the "equivalent albedo A_0" corresponding to craters, elevations and relatively flat surfaces which have been chosen on the lunar map or examples for this report. The comparison of the A_0 with terrestrial samples, however, will not be attempted here because of the differences between the "equivalent albedo" and that obtained from earth-based observations. In addition, a brief critical examination will be made concerning the laboratory method used for measuring albedos of terrestrial samples.

Chapter 2

PRESENTATION OF THE RESULTS OBTAINED FOR THE "EQUIVALENT ALBEDO A_0"

To study the variation of "equivalent albedos" in craters, a region of the moon with a quantity of major craters has been chosen in order to better determine the differences in albedos. In other words, it was convenient to choose a zone presenting good contrast between craters and relatively flat surfaces and between these relatively flat surfaces and other elevations. The areas were chosen for the study with respect to the selenographic longitude of Surveyor in Western and Eastern Hemisphere sides of the spacecraft, 25° relative longitude and a range of from 0° to $\pm$12° latitude. For the discussion of the results obtained concerning the "equivalent albedos A_0", those values relating to the Western Hemisphere only are graphically represented However, complete discussion is given of the values corresponding to the Eastern Hemisphere and the lunar relief considered for this is indicated in Figure 14.

As shown by Scheme VIIa, the size of craters has been arbitrarily defined with the adjectives "minute, very small, smaller, small, medium, large, larger and largest". The minute crater is defined in this report as the least visible point seen with a magnifier on the lunar map used. In other words, the diameters given in Scheme VIIa for the craters correspond to the difference read on the reference map between the Western and Eastern borders of craters; such difference for the diameters has been calculated in minutes of arc and translated into miles. This latter dimension has been derived by adopting a lunar diameter equal to 2,160 miles. Following

the instruction given in step 3 of the Procedure for Obtaining Albedos, the $\widehat{\delta T_0}$ values have been deducted from the effective temperature contour transparent master in the following way.

As indicated in Scheme VIIb, T_0' has been first read from the North to the South and then from the East to the West. However, to obtain optimum precisions of readings, additional T_0' values have also been read from NW to SE and from NE to SW . In this manner, a first differential was obtained with the integration of values N → S and E → W while the second differential was obtained with similar integration of values NW → SE and NE → SW . A mean for $\widehat{\delta T_0}$ has been adopted from these two differentials. Also, to define as well as possible the temperature variation on the surrounding neighborhood of craters, the readings of T_0' were made one degree beyond the rims in longitude and in latitude. This procedure enables the discrimination of the temperature values corresponding to craters varying in size. For the larger categories of craters, containing an extension of relatively flat surface and small elevations inside, the following procedure was followed:

1. Considering the center as a point on the relatively flat surface, the T_0' values were read, as indicated above, going from one degree beyond the rims, through these rims, to the center of the crater.

2. For the rims, as well as the small inner elevations, the T_0' values which correspond to the top and to the bottom of the craters were considered as a function of the width indicated on the lunar map used.

3. After establishing the differences between relatively flat surfaces and elevations, a final evaluation was made of the $\widehat{\delta T}_0$ average by taking into consideration the inner depression of the crater. This final evaluation is the $\widehat{\delta T}_0$ adopted for the center.

4. As indicated in Scheme VIId, a number of circles for the T_0' in the case of craters with extended and nonextended rims were considered.

For a total of 412 craters in the Eastern Hemisphere of Surveyor, the results relating the "equivalent albedos A_0" of crater centers are presented in Table 3. In order to better follow these craters when examining Figure 14, their enumeration in this figure is repeated in the first column of Table 3. This column is followed by a second column giving the corresponding arbitrary definition of diameter, shown in Scheme VIIa. In the same manner, their respective selenographical coordinates have been added. The fifth column gives the slope, n/N, while the sixth gives the T_0' obtained for the vertex of craters. The lunar material absorption is given by the seventh column and the last column gives the "equivalent albedo A_0" as obtained from equation (14). The word "range" used in that last column indicates that the A_0's have been obtained according to step 3 mentioned above. Finally, the names of some known craters have been indicated.

Results are given in Table 4 for topographic elevations. The definition adopted here for elevation is any kind of lunar feature which rises above the relatively flat surface level, including rims of craters, ridges, small hills and mountains. Some of the crater rims are specifically mentioned in Table 4

in order to study the differences in composition, if any, of the major craters located in the Eastern Hemisphere of Surveyor. With regard to the relatively flat surface, the lunar areas have been selected to avoid, as much as possible, clusters of very small craters; also, areas where small ridges are suspected to be present were avoided. An example of this procedure is mentioned in Figure 14, point N°41 . The results pertaining to the relatively flat surface are given in Table 5.

The graphical representation of "equivalent albedos" for the center of craters is given in Figure 10. The ordinate of this figure represents the percent of such albedos while the abscissa represents the corresponding percent of the absorption $(N/\eta) \cdot \widehat{\delta T}_0$. As indicated on Figure 10, many of the figures representing the results are not placed on the exponential curve. The curve is not large enough to contain all results from the 412 craters studied. This is also the reason why many values for craters have been placed in their corresponding range of variation instead of their exact position on the curve. Concerning the relatively flat surface and elevations, the graphical representation of their values is given in Figures 11 and 12, respectively. However, in the case of the relatively flat surface, only the range $0.300 < A_0 < 0.700$ is graphically represented in order to keep the ordinate scale used in the other figures.

In order to facilitate this discussion, two extreme cases found for craters and relatively flat surfaces during the first analysis of the Orbiter's photographs are explained. The first of these cases concerns some of the small craters situated on a relatively flat surface. Their "equivalent albedos" are found to be almost equal to 100%. The notation

Some examples of the Cases A_r and A_s are shown in the illustration below.

A_r : the close neighborhood of small craters is too bright.

A_s : the neighborhood is darkened.

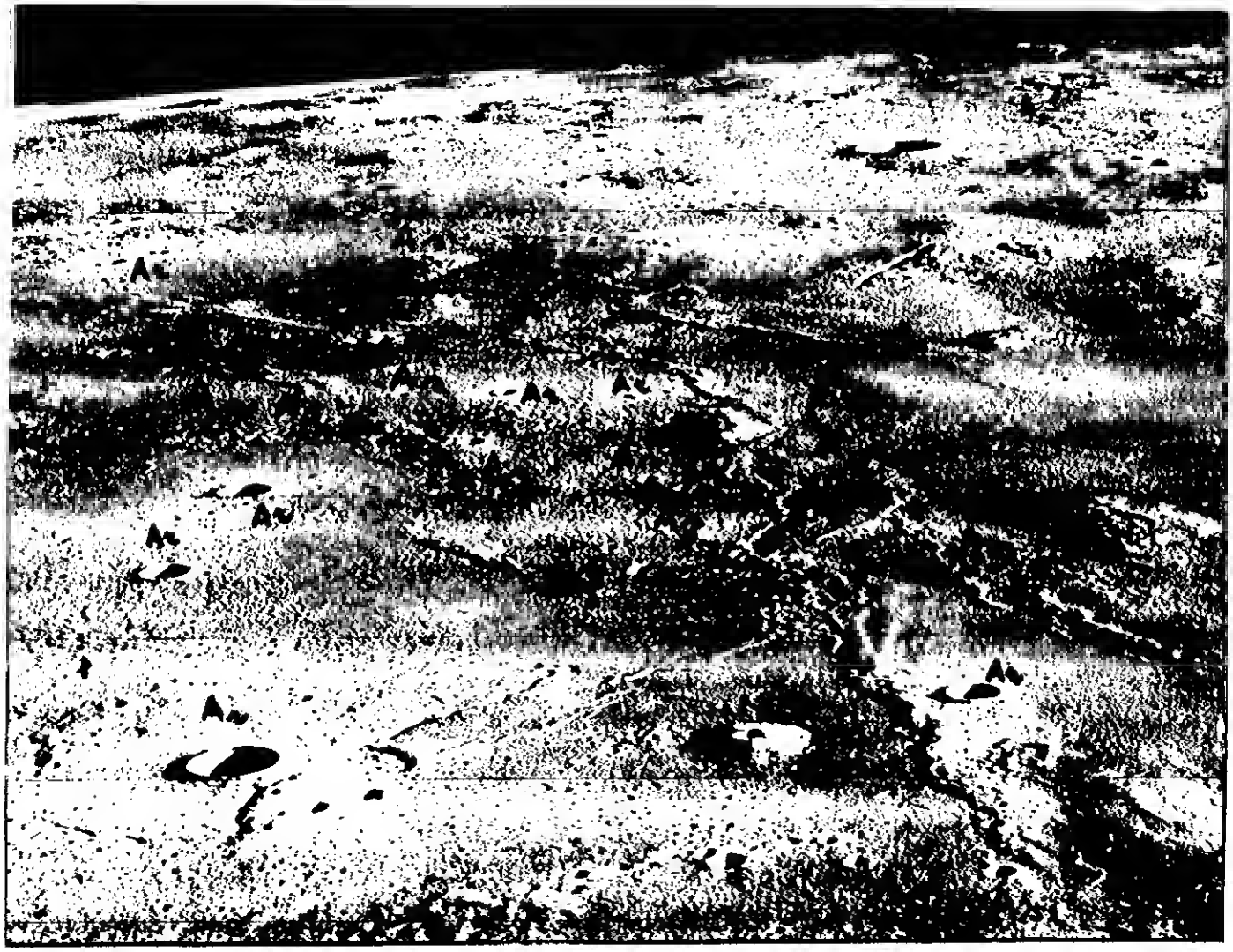

is simplified by writing: $A_r/100 \cong (N/n) \cdot \delta\hat{T}_0$. The A_r is to distinguish this particular value of A_0 and the symbolic equality indicates that the absorption is reaching its minimum. The other case concerns the relatively flat surface close to small craters which can be expressed: $A_r \cong A_s \cong (N/n) \cdot \delta\hat{T}_0$. The A_r being the value already mentioned, A_s is the notation used to distinguish the A_0 corresponding to this second case from the first one. The symbolic equality means that both A_r and A_s are reaching the same minimum as the absorption.

The picture above shows some examples of the two cases, A_r and A_s . This picture is a reproduction of an Orbiter II photograph showing a large area of the crater Marius on the lunar horizon. The eastern neighborhood of this area of Marius is not too far from the landing site selected from the slope suggested by Figure 1 in the first report, taking as reference the site where Surveyor landed. The contrast of the photograph is good enough to show clearly the two cases, A_r and A_s . The craters indicated by A_r are too bright in comparison with the next surrounding area. With regard to the points A_s , the figure shows that the relatively flat surface near the craters seems to be very dark in comparison with the subsequent darkening due to the shadows on areas close to small hills and ridges. Both cases are abundant only in areas where the effective temperature contours show irregular shapes.

Chapter 3

ANALYSIS OF THE "EQUIVALENT ALBEDOS A_0 " OBTAINED

In Figure 10, the A_0 obtained for the centers of craters provides interesting information about the distribution of craters. Upon examination of the lunar map of Figure 14, one notices: (1) The major and other significant craters do not seem to be randomly distributed on the surface. Although it is difficult to well define such a distribution, the general impression is that the distribution of craters appears to follow an exponential curve which is also followed by other less important craters in size as well as in shape. (2) The range size of craters going from "minute" to "smaller" does not seem to follow any definite distribution. In this regard, one notices only that the sizes ranging from "very small" to "smaller" craters are often grouped around the bigger ones; one sees them in a relatively abundant quantity between mountains or forming a chain with ridges. (3) "Minute" craters are randomly distributed across the relatively flat surfaces of the moon.

The A_0 of Figure 10 shows a very neat distribution of lunar craters. Such a distribution can be described in the following way: (1) There is a family of craters composed of groups I, II and III. In this family, the inner material of craters is reflecting more sunlight than it is absorbing and the quantity of reflected sunlight is increasing very fast from the craters of group II. There is a very slight separation between the end of group IV and the beginning of group III, but this separation is very neat between the groups III and II and also between II and I. Most of the craters

forming this family belong to group III. However, there does not appear to be a significant difference in this regard between the other two groups. (2) Another family is formed by groups IV, V and VI. In this case, the inner materials absorb more sunlight than is reflected and the quantity of such absorbed sunlight varies very slowly from one group to another. The separation is neat between them and, from the quantity point of view of craters forming groups in this family, it appears that group VI is smaller than the other two groups.

For the Eastern Hemisphere of Surveyor shown in Figure 14, an example of the distribution mentioned above is prepared as follows:

First Family

Group I : Kepler C.

Group II : Kepler.

Group III : Copernicus; Kunowsky and Kunowsky D; Encke C; Hortensius B, D and s; Kepler D; Lansberg K, R and m; Reinhold 8 and 10.

Second Family

Group IV : Encke and Encke B; Reinhold and Reinhold t; Maestlin; Lansberg and Lansberg A, A_{30}, B, F and o; Kepler A, A_0 and B; Copernicus N, 20 and 27; Hortensius A and r; Kunowsky C and C_0; Gambart AC and AS; Fra Mauro t.

Group V : Fauth; Hortensius and Hortensius E, r and s; Encke 3 and D; Reinhold A, N and 24.

Group VI : Lansberg C and 24; Hortensius 0 and o; Reinhold K.

Figure 10 shows the case $(N/\eta) \cdot \hat{\delta T}_0 \cong A_s \cong A_r$. The values corresponding to some examples for this case are indicated with the same oval as was done previously in Table 3. Also, Figure 10 shows the example represented by crater 2 for which the A_0 is relatively high. However, this is due to "minute" craters, such as No. 2, randomly distributed on the relatively flat surface of the moon.

In Figure 11, one sees that the variation of A_0 is less pronounced in the case of elevations than it is for craters. Examination of Figure 11 shows this variation of A_0 which can be summarized as follows:

Part A: The quantity of reflected sunlight almost equals that which is absorbed. Also, from one extreme to the other of Part A, this variation is almost inversely related to both A_0 and $(N/\eta) \cdot \hat{\delta T}_0$. Some crater rims with this characteristic are Kepler, Lansberg A, Hortensius A and Hortensius r.

Part B: The quantity of reflected sunlight is greater than that absorbed and A_0 varies faster than $(N/\eta) \cdot \hat{\delta T}_0$. Examples of crater rims with this characteristic are Encke B, Kunowsky, Kepler D, Reinhold A and Encke.

Part C: The quantity of the reflected sunlight is greater than that absorbed. However, the variation of A_0 with respect to $(N/\eta) \cdot \hat{\delta T}_0$ is slightly faster. Examples of crater rims in this case are Reinhold, Lansberg, Copernicus and Fauth.

Part D: The quantity of reflected sunlight reaches its minimum; also, $(N/\eta \cdot \hat{\delta T}_0$ has very small and slow variations. The rims of Maestlin belong to this case.

Concerning the relatively flat surfaces, the quantity of reflected sunlight is too great and varying too fast when compared with the quantity of sunlight which is absorbed by the lunar material. For values of A_0 higher than 35% and approaching the case A_r, previously mentioned, the relatively flat surface of the moon seems to reflect the sunlight as if it were made up of metallic materials which formed a "somewhat compact layer". With the term "somewhat" one means that such a layer could have a good bearing strength in some areas while in other areas it could have a weaker bearing strength because of local temperature factors. Such a layer might explain why the quantity $(N/\eta) \cdot \hat{\delta T}_0$ reaches its maximum so quickly when $A_0 \approx 35\%$. Also, besides the grain size variation of such metallic materials, other types of variations in the range $35\% < A_0 < 100\%$ could be due to the presence of any kind of small lunar relief able to cause slight absorption of the sunlight.

In this respect, for example, the case of points 6, 10 and 12 are cited in Figure 12. These points are not too far

from the site where Surveyor landed. The lunar map of Figure 14 shows that these points are close to a ridge; in the same manner, the points 8 and 11 of that area are right on a very small elevation. A similar comment that one can make from Figure 12 concerns the points 22, 23, 24, 25, 26, 29, 30, 31, 32, 33, 34, 35, 36, 37, 38, 39, and 40. All these points are situated in an area where small ridges, craters and elevations are present. With respect to the point 41, it has been explained already why such a point has been taken in an area other than that previously considered in Figure 14.

From this analysis of the "equivalent albedo" obtained from the T_0 furnished by Surveyor, it appears that one must be very cautious in reaching conclusions about the lunar surface composition when comparing albedos of terrestrial samples with the standard lunar photometric contours. On one hand, earth-based observations are only based on the reflected sunlight to obtain information about the lunar albedos. However, we have seen how the reflected sunlight is altered. Because of this troubling factor, it is very difficult to determine with good accuracy the real characteristics of the albedos corresponding to the different lunar features. On the other hand, it appears also that one physical parameter is not enough to tell about the nature of a given body. In other words, in utilizing comparisons with the standard lunar photometric contours to determine accurately the composition of the lunar surface, it is necessary to do the following: (1) Define the reduction techniques of observational data to clearly discriminate the albedos of the different lunar reliefs. (2) Consider the fraction of sunlight absorbed by the lunar surface

feature in question. (3) Make measurements in the laboratory of both physical parameters with terrestrial samples. (4) Proceed to the joint comparison of the determined measurement with those data corresponding to the lunar observations.

Chapter 4

COMPARISON BETWEEN OUR PRESENT KNOWLEDGE ABOUT THE LUNAR COMPOSITION AND THE SIMILAR INFORMATION OBTAINED FROM THE USE OF "EQUIVALENT ALBEDOS"

The composition of the lunar surface has been previously studied mainly by using the lunar-optical scattering law. However, the results obtained from this study are not satisfactory, as yet, for reasons which can be summarized as follows: (1) The lunar-scattering law has been established in a very empirical way, that is, without first establishing in a precise manner the different characteristics of lunar topography. (2) It has been the tendency in the past to define the scattered light of a body as a function of one, two or even three physical parameters and by separately considering each of them. However, from the previous explanation, it is indicated that the light scattered by lunar material cannot be defined as a function of an individual physical parameter because all possible factors play their role simultaneously in a given area.

The discrepancies from the comparison of albedos obtained from earth-based observations and those obtained from terrestrial samples studied in the laboratory are sometimes due to the method adopted for establishing such a comparison. For instance, the representation of earth-based observational data of albedos in the form of a polar diagram of reflectivity, which is also known as the diffusion function, gives a group of curves extremely extended in the direction of the sun for any angle of incidence of the solar rays. When this procedure is followed, it appears that the curves corresponding to the maria are similar to those corresponding to the elevations. As a result,

the conclusion has been that the surface of the moon is covered by an extremely porous matter similar to a slag or a spongy structure.

The comparison between the sunlight reflected by the lunar surface and that reflected by different artificial models and terrestrial samples has been based on a reflection law defined by a very empirical method. In effect, such a method consists of a photometric comparison of the determined reflection law for the moon and for those objects under test. This comparison is done in two different ways: (1) The brightness of the lunar surface coefficient is obtained as a function of the angle of incidence for solar rays, the angle of reflection and the phase angle. (2) The lunar-surface brightness coefficient is then compared with the brightness coefficient obtained for terrestrial samples. However, this method is already limited due to the fact that the lunar surface coefficient variation is established from empirical methods. As a result, the range of possible values of reflectivity is severely limited for each particular region of the lunar surface.

The method using the indicatrix of scattering is inconvenient. In the first place, the comparison of scattering indicatrix of the lunar surface with those of terrestrial formations assumes that a general mean indicatrix can be photometrically obtained for the moon by comparing it with supposedly similar terrestrial materials. However, because of the particular conditions of observation of the moon, it is not possible to determine scattering indicatrix from earth for any sector of the lunar surface. Secondly, lunar objects could be observed from a single angle of view, and with limited

combinations of angle of incidence and azimuth of the incident ray, which can be determined from the position of the lunar object observed on the disk of the moon. There is also the difficulty of making appropriate identification and fixation for separate sectors of the lunar surface when observing them by visual photometers, especially when the assumption is made that the light scattering law is the same for all lunar objects observed. Or to put it another way, the errors committed when measuring the relatively flat surface of maria could be small; however, these errors would be considerable for those elevations which might have, photometrically speaking, a less homogeneous structure.

It must also be pointed out that a very unusual scattering property has been attributed to the moon. Some authors think that the large backscatter could be produced by corner reflectors or transparent spheres of proper refractive index. However, such structures are obviously artificial and contrived, inasmuch as they would have to cover the entire lunar surface and would not endure long under micrometeorite bombardment. Another explanation for the peculiar photometric behavior attributed to the moon is that it results from shadows cast by an intricately structured material lying on the lunar surface. This hypothesis also claims that the structure into which this material is arranged is large in comparison with a wavelength of visible light, since objects comparable with or smaller than a wavelength forward-scatter light and a narrow backscatter peak would be impossible. The conclusion that results from these theories is that the surface of the moon must be covered by an optically thick layer of extremely rough material with irregularities of size between 10μ and 1 cm .

The investigations undertaken in the laboratory show that the photometric properties of the lunar surface correspond to terrestrial samples such as rocks, sands, lavas, volcanic ashes and meteorites. The major difficulty found for these materials is that none reproduce exactly the lunar reflection law. Many authors explain this by stating that the lunar surface has been exposed to a type of weathering far different from that to which terrestrial rocks have been exposed. Other investigators think that bombardment by micrometeorites and solar corpuscular radiation should alter the optical properties of minerals appreciably. However, the terrestrial samples could reproduce the lunar reflection law if one had the capability to perform the laboratory experiments under the same conditions as those of the moon. The most accurately obtained only take into consideration the albedo, the optical scattering characteristics of the individual objects of which the surface is composed, and the type of structure in which the objects are arranged.

Let us now consider the following questions: Since we must be cautious when making conclusions from earth-based observations, then what would be the most appropriate way to get information about the real composition of the lunar surface? For example, is there a general composition for the whole lunar surface or has each lunar relief its own characteristic composition? There is no doubt that, with regard to the first question, the best lunar observations should be done out of our atmosphere. With regard to the second question, the writer has attempted to obtain necessary information by examining the variation of behavior of the quantities A_0 , $(N/\eta) \cdot \hat{\delta T}_0$. For each of the lunar relief features considered

in this report, the graphical representation of such a variation of behavior is done within Figure 13. The abscissa represents the absorption $(N/\eta) \cdot \hat{\delta T}_0$ while the ordinate represents the "equivalent albedo A_0".

Each of the exponential curves shown in Figure 13 is the mean of results obtained, respectively, for craters, elevations and relatively flat surfaces. The first impression that one gets from Figure 13 is that there is not a general composition for the whole lunar surface but rather a characteristic composition for each of the lunar relief features considered. However, judging from the evolution of each of such exponential curves, one gets the impression that the composition of relief seems to be much more related to the factors influencing the evolution of the original features rather than to be strongly influenced, or modified, by factors such as the solar corpuscular radiation or by changes resulting from bombardment of micrometeorites.

The variation of behavior in Figure 13 can be described as follows: (1) The variation of both quantities A_0 and $(N/\eta) \cdot \hat{\delta T}_0$ is well defined in a certain range for each of the lunar relief features considered. The determined range is about $0.01 < A_0 < 0.30$ for reflected sunlight by the lunar craters, about $0.01 < A_0 < 0.10$ for the elevations and about $0.15 < A_0 < 1.00$ for relatively flat surfaces. (2) There is a discontinuity between elevations and relatively flat surfaces between $A_0 \approx 0.10$ and $A_0 \approx 0.15$. This discontinuity indicates that the relatively flat surfaces in the vicinity of elevations become highly absorbant of the sunlight. (3) The lunar craters, in the range already

mentioned, are at the same time more absorbant and more reflectant material of sunlight, within the same range of A_0 , than elevations and relatively flat surfaces. In effect, when $A_0 \approx 0.30$, their exponential curve tends to conform to that of relatively flat surfaces. Since the value $A_0 \approx 0.30$ corresponds to very small craters, then the said tendency means that craters smaller than this, i.e., "very small crater category", also have their absorbant and reflectant properties conform to that of the lunar area where they exist.

From this comparison between our present knowledge about the lunar composition and the same information determined from earth observations, we see that improvement must still be made on studies based on the application of the lunar optical scattering law or through use of indicatrix of scattering. Another important question is to know the eventual differences in albedo, in a given point of the lunar surface, when removing the loose surface material. In the point where Surveyor landed, for example, the scene luminance was measured for parts of the lunar surface surrounding the pad upon which the photometric target was mounted. By fitting the measured scene luminance to the photometric function from the telescopic measurements of Fedorets, an estimate of 9% for the normal albedo was derived for the parts of the surface which appeared to be undisturbed by the pad. The estimate albedo for the disturbed areas was about 3% lower. However, the scattered light from the spacecraft has been a particular problem in evaluating the luminance on the lunar surface. There is no doubt that the direct determination of the scattered light from the Orbiters' photographs is necessary to get more precise information about the lunar surface composition.

Chapter 5

CONSIDERATIONS FURNISHED BY THE "EQUIVALENT ALBEDOS" FOR ANALYZING THE LUNAR SURFACE PHOTOGRAPHS:

From the variation of behavior of the "equivalent albedos" which has been previously described, we have determined certain values of A_0 which seem to indicate that the moon is not a "dead body". The moon seems to contain some areas which might be dangerous for the astronauts. Examples of such peculiar values of A_0 are the two cases, A_r and A_s, and some craters which will be examined in greater detail in the final part of this report. Since the astronaut is supposed to do some lunar exploration at the landing site selected from earth, then we must determine, in advance, if a selected area could have small regions dangerous for landing. With this information, and in view of the fact that the astronaut must, while in flight, identify the area of interest, we can define the minimum requirements of the equipment carried for the tracking operation.

From the analysis of the Orbiters' photographs we require the following additional information: (1) Definition of the lunar exploration the astronaut is to conduct. (2) Definition, before determining lunar slopes from the photographs, of the problems which result from the attenuation of reflected sunlight by our atmosphere when comparing albedos using the lunar photometric function method. To analyze for the dangerous points in a supposed safest area, it is first necessary to examine all available lunar photographs in order to extend the knowledge so acquired to the whole lunar surface. This means that an examination must be made of all Ranger, Surveyor and Orbiter photographs at our disposal. In effect, dangerous points in a supposed safest area could have their origin far from the area under examination.

First, we must consider the degree of lunar coverage accomplished per flight, the extent of the lunar surface spectrally analyzed and the suitability of the results for correlation with data obtained from other remote sensing experiments. Thus, the analysis of pictures represents an integrated and complementary photographic package, with respect to spatial and spectral resolution and coverage, to better discriminate the dangerous points within the area studied. Of course, the work must be complemented with measurements on the photographs. Size, shape, texture and configuration of the lunar surface features to determine the local and regional variations in the spectral reflectivity and emissivity of the lunar surface must be determined. For this purpose, one can use the wavelength range from 2000Å to 1.1μ in the imaging systems, and the ranges from 1000Å to 3000Å and from 1μ to 20μ for the non-imaging systems. In regard to the overall scientific information which must be furnished to the astronaut prior to the launch, the check of the results of analyses should be done as follows: (1) After establishment of controls for lunar geodetic surveys, identification of peculiar points within new lunar topographic maps should be produced through use of metric and panoramic photography. (2) Final identification and discrimination of lunar features should be made utilizing high resolution and multiband synoptic photography. (3) Application of (2) with regard to peculiar lunar features within ultra high resolution photography coupled with multiband remote sensing. Checking will be much easier to accomplish with new experiments expected from the next Surveyor.

Secondly, we must consider the observational equipment to be carred on the manned spacecraft in the specifications

to be furnished to NASA. In other words, the most convenient camera system and individual components should result from knowledge acquired from the analyses of Ranger, Surveyor and Orbiter photographs. From these analyses, specifications resulting from preliminary estimation would be as follows: (1) A system operating in two modes, imaging and non-imaging, will be necessary. The primary system should be a telescope of about 16" aperture which, by use of beam splitters, would form a number of separate images. Because of the dual requirements of image motion compensation and long integration times, this telescope should be appropriate for efficiently tracking the target. From examination of the first Orbiter III photographs which have been made available, the 16" aperture telescope must be linked to the viewfinder so that the astronaut can easily identify the area of interest within the ultra high resolution system. The next Surveyor scheduled for April 1967 could give us more information about points (1) and (2).

Concerning the photometric and other photographic characteristics required for geologic study and mapping prior to the launch of the manned spacecraft, the first task should be to do the specific earth-based observations suggested by the "equivalent albedos" results presented in this report. The identification and discrimination of the two cases, A_r and A_s, is easy to do when using the procedure developed by the successive transformations of observational data. For example, if we assume that eventual landing sites are selected on the Eastern Hemisphere of Surveyor shown by Figure 14, promptly we would see that the peculiar points already cited are situated in Figure 15 in areas where the Effective Temperature Contours show irregularities. In effect, besides the examples graphically represented with ovals in Figure 15, all convergences of contours or shapes other than straight lines indicate the presence of such peculiar points. Thus,

as indicated by Figure 15, it is necessary and sufficient to place the transparent master of Effective Temperature Contours over the lunar map for the area of interest, to quickly identify and discriminate the points corresponding to the cases mentioned above.

However, as previously pointed out, the analysis of earth-based observational data within the Standard Lunar Photometric Contour still has to be perfected. This is especially true to establish the effect of the attenuation by our atmosphere on the reflected sunlight. Also, we can see in the example in Figure 16 the atmosphere absorption effects shown by the comparison between the "equivalent albedos" and the said lunar photometric contours. Since the observational brightness is referred to the standard brightness of an ideal white diffused reflector under the same conditions of illumination, the albedo determined in this way does not eliminate, completely, the error introduced by the earth atmosphere on the intensity of the reflected sunlight. Thus, when observational data minus observational errors are divided by a constant, the result is that the corresponding albedo's curve is higher than the real albedo's curve of reflected sunlight before penetrating our atmosphere. The atmosphere refraction effects are not well defined as yet in the method using the lunar photometric function. (The abscissae given in Figure 16 for the Standard Lunar Photometric Contour will be explained later.)

This first comparison between both exponential curves in Figure 16 shows that, with new improvements, the method using the Standard Lunar Photometric Contour is adequate to measure slopes from the lunar surface photographs. As will be seen in the next section, such a method is even to be recommended when jointly used with the exponential

curve of "equivalent albedos" for testing slope measurements. This is just what is needed since the arguments used against the method cited is that there has been little opportunity to check its validity. In other words, with the Ranger, Surveyor and Orbiter photographs plus the "equivalent albedos" resulting from this research there is now a good opportunity to use it with confidence. One can say that the first thing to do is to eliminate the normal errors introduced in the definition of the photometric function. In the same manner, the way to determine albedos must be reviewed, especially the methods of data reduction, so that consideration of other factors such as the lens transmission and illumination values can be made.

Chapter 6

THE USE OF "EQUIVALENT ALBEDO" AND STANDARD LUNAR PHOTOMETRIC CURVES FOR MEASURING SLOPES FROM LUNAR SURFACE PHOTOGRAPHS, ABSORPTION EFFECTS

Of all the problems involved in utilizing the present state of the Standard Lunar Photometric curves, perhaps the most important is the alteration of reflected sunlight by our atmosphere. In this respect, the biggest uncertainty in using it comes from the fact that one cannot accurately discriminate the different albedos of the lunar relief features. Among the complicated factors to consider in earth-based observations are image distortion and the variable attenuation of the radiation's intensity which must be considered in the following way: (1) Define the techniques of photometric observations to eliminate as nearly as possible the effects of atmospheric tremors. For example, when observing a small area of the moon, the oscillation of the image that falls on the entrance aperture of the photometer must be eliminated. (2) Eliminate the light contamination effects. For a given small area of the moon observed, the light contamination coming from adjoining areas is introduced into the signal and its amplitude varies with the quality of the viewing. In such a case, the photometric accuracy desired depends on the general nature of the local region observed on the moon. As a result, good accuracy can be obtained by determining the optimum size entrance aperture on the photometer as a function of the steadiness of the image.

The analysis shown in Figure 10, 11 and 12, reveals that the light contamination from surrounding areas would be less important in earth-based observations if the lunar surface of the same topography is considered separately. However,

such contamination always is important in the category of "large, larger and largest" craters and it is caused by the inner relatively flat surface; in the same manner, it is important in extended relatively flat surfaces which have significant groups of "smaller, small and medium" craters. It is recommended that, when observing specific areas of landing sites selected by NASA, the larger aperture size of the photometer should be used during nights of large image excursion. As a consequence, the light contamination would be held to a level below a 5% accuracy on the photometric measurements. However, for the lunar areas where the contrast among features is important, the lowest light contamination level can be obtained by establishing the mean of separate observations of such features.

Also, since the observation of landing sites selected by NASA concerns specific lunar areas, another recommendation is to eliminate the light contamination effects caused by the telescope guiding errors. In this respect, and since a given slit width required increases as the photometric tolerances become more stringent and seeing amplitude gets larger, the effects would be considerably diminished by observing with small slit width each time the intensity differences of contrasts are small in the lunar regions observed. With regard to image distortion, the problem is accentuated in the sense that the attenuation caused by our atmosphere varies with the wavelength and observing time. For example, in the range $0.4\mu \rightarrow 2.5\mu$ most of the absorption is due to water vapor, with several "windows" ocurring in this region, and the intensity of the absorption in these regions is a function of the water vapor content of the atmosphere.

Because of this, it is difficult to determine with accuracy the earth atmospheric absorption coefficient. Still other troubling factors are the air mass variation in latitude and altitude of the observing site, the more complex variation of the overlying air mass with temperature, degree of humidity, zenithal distance of the moon, atmospheric turbulence, etc. These make it much more difficult to obtain a good accuracy on the determination of the coefficient already mentioned.

From the reasons explained, one sees that a final earth-based data "observed reflected light intensity plus atmospheric attenuation" never exactly reproduce the real intensity of the reflected moonlight before penetrating our atmosphere. A first comparison between exponential curves of "equivalent albedo" and Standard Lunar Photometric Albedos cannot agree in spite of corrections made on observational data. This can be noticed in Figure 16 by observing that the Standard Photometric Albedos are still greater than those of other exponential curves. These Standard Lunar Photometric Albedos represent a mean established from observations made by Fedoretz, Minnaert and Gehrels; Orlova and Van Diggelen established the said mean after analyzing data corresponding to a great number of crater floors, maria and continents distributed widely over the lunar disk. The average measurements of such lunar features are presented as brightness versus phase curves for longitudes 0°, 30° and 60°. The zero of said longitudes, which are also named "viewing angles E," corresponds to the apparent center of the lunar disk.

The additional abscissa axis of Figure 16, which was explained earlier, is necessary for the comparison that we

discuss here because of the different definitions between the Standard Lunar Photometric Albedos and A_0 . In other words, since the absorption of the reflected sunlight by the lunar material is not represented in the Standard Lunar Photometric Contour, for the said comparison, it has been necessary to proceed as follows: (1) For both hemispheres of Surveyor which have been previously described, and for some points considered in this report but included in the observations of Fedoretz, Minnaert and Gehrels, one has taken the corresponding cosine of the viewing angle E; this data $\cos E$, is affected by a factor of 10 in order to match the scale adopted in Figure 16. (2) Since earth-based observations albedos are with respect to A_0 , the remaining quantity of sunlight which is reflected after absorption, then the additional abscissa represents the said quantity of light $(N/\zeta) \cdot \delta T_0/10 \cos E$ left free and reflected by the lunar material at the point considered the moon surface. (3) To keep the working style of this research, one has adopted the longitude of Surveyor as reference instead of that corresponding to the apparent center of the lunar disk. (This is indicated in Scheme VIII, where some points considered in Figure 14 for the Eastern Hemisphere of Surveyor are also mentioned.)

Before further discussion and for the sake of clarity, it would be convenient to recall briefly the following facts: (1) The exponential curve of A_0 used in the comparison is a mean established from Figures 10, 11 and 12; the only difference is that the discontinuity between the relatively flat surfaces and elevations has not been taken into consideration. (2) However, on the exponential curve of A_0 shown in Figure 16, it has been indicated where discontinuity occurs. The maximums found on the curves correspond to

craters and elevations, and the minimum corresponds to the relatively flat surfaces. The agreement is good between the two curves in the case of relatively flat surfaces and elevations; this is because the light contamination is less important in earth-based observations corresponding to the lunar areas with almost constant topography. The agreement disappears little by little as the light contamination caused by significant groups of "smaller, small and medium" craters becomes important. However, there is no agreement for other size categories of craters bigger than those already cited; this is due to the light contamination coming from relatively flat surfaces inside significant craters.

We see that agreement sought from direct comparison between "equivalent albedos" and Standard Lunar Photometric curves can be summarized as follows: (1) Correlation between earth-based observational albedos and A_0 ; this means that the observational albedos must be considered with respect to A_0 as the quantity of sunlight left free and reflected by the moon at the point considered. (2) Correction of observational data of the light contamination effect; this correction must be separately done for each of lunar relief features. Figure 16 contains an analysis and discussion of points (1) and (2) from which one can reach the following conclusions: The agreement is good concerning the comparison established in point (1). The light contamination effects of point (2) persist in the case of craters; such an effect becomes less and less important with the presence of groups of "smaller, small and medium" craters and becomes markedly strong in the case of significant craters.

The light contamination effects should be analyzed by comparing only the Standard Lunar Photometric contours with the exponential curves for craters. This has been done in Figure 17 and it appears that this comparison would give a best fit if our atmosphere were able to discriminate clearly the sunlight reflected by the inner relatively flat surfaces and rims of significant craters. In order to resolve the problem graphically illustrated in Figure 17, let us consider in SCHEME VI the arbitrary position P' which is opposite P . As it is better shown in SCHEME IX, let us consider the imaginary triangle SUN-MOON-P' instead of that SUN-MOON-P. The previous analysis of the reflected sunlight will be imaginarily done at P' , where there is no question about any atmospheric disturbance. With regard to the connection between the practical point of view and this other analysis, let us proceed in the following way:

(1) Determine from the lunar ephemerides the angle i corresponding to the position A of the moon, as shown in SCHEME IX. (2) For that ephemeric data, and after correction of the atmospheric refraction coefficient corresponding to the divers factors described by the refraction laws, determine the angle h between the reflected sunray and that coming directly from the sun toward the earth. (3) Check the values of $\hat{h}$ and $\hat{i}$ by taking into consideration the angle j between the sunray going to the moon and that coming toward us (after have made for $\hat{j}$ the same type of correction for the atmospheric refraction coefficient). (4) Since the summations of $(\hat{h}' + \hat{i}' + \hat{j}' = 180°)_p$, and that of $(\hat{h} + \hat{i} + \hat{j} \approx 180°)_p$, establish the difference between both summations to get the coefficient defining the deviation

caused by our atmosphere on the direction of the reflected ray of SCHEME IX. (5) To assign such a coefficient to the value of the viewing angle E as a function of that of $\hat{i}$ previously determined in (1).

In this way, if our atmosphere is not able to clearly discriminate the light contamination effects when observing different features of a given lunar area, we have at least now a new coefficient which defines the real direction that a given reflected sunray had before penetrating the earth's atmosphere. With the knowledge of the absorption by the lunar material of the sunray before reflecting it and that deviation coefficient already cited, it is possible to obtain a mean profile between two curves which can serve as reference for checking earth-based observational data. As is shown in Figure 18, the agreement between said curves is reached with the new abscissa axis $(N/\zeta) \cdot \delta\hat{T}_0/3/5 \cos E$ when $E < 45°$, or $(N/\zeta) \cdot \delta\hat{T}_0/3/5 \sin E$ when $E > 45°$. This coefficient 3/5 is a mean established from the same observations made by Fedoretz, Minnaert and Gehrels and corresponding to the points considered in this research. However, if a perfect fit of the curves in Figure 18 is preferred, instead of a mean profile, then it is recommended that the operations described above in (1), (2), (3), (4) and (5) be repeated for at least 3 different positions of the moon, such as A, A', A'' in SCHEME IX, during a same observing night and, better yet, to make the observations on three nights. Then the final plot in Figure 18 would be done with the mean from the 3 values of the atmospheric refraction coefficient.

As a conclusion, the fit above between the "equivalent albedo" and the Standard Lunar Photometric curves constitutes

a good method for precisely measuring slopes from lunar surface photographs to overcome the lunar area considered under two different illumination conditions, preferably with opposite phase angles. With regard to the albedo determinations from Orbiter photographs, it would be advisable to first correlate the stereo compilation and the photometric reduction with the low resolution photography and extrapolate the results to high resolution image. After this, the albedos obtained can be analyzed within the explanation of Figure 18. This type of analysis will provide valuable information for cartographic support at a time in which all data reduction tools will be pressed to their limits.

Chapter 7

CRATERS WHICH APPEAR INCONVENIENT FOR BEING EXPLORED BY THE ASTRONAUT

The Ranger, Surveyor and Orbiter photographs do not indicate any unduly hazardous aspects of the lunar craters which cause astronauts to avoid them; on the contrary, they appear as inactive craters on the lunar photographs. The difference in albedo A_0 from outside to the craters' centers, however, shows that some of them are not "dead craters" and that their distribution on the lunar surface is related to the origin and evolution of the groups established in Figure 10. As described previously, such distribution was found with characteristics similar to that defined by exponential curves. In a similar manner, it has been found that origin and evoluation of these groups arise from the existence of two families of craters; these two families appear different. In order to define the lunar explorations that the astronaut is supposed to do, let us discriminate the inconvenient craters in the following way:.

The gradual change in albedo along a line from a point outside of a crater to the center of a crater, as shown in Scheme VII, may be measured for all craters situated within the ridge-rimmed elliptical area where Surveyor landed and may be compared with that of Flamsteed. This has been done for the lunar areas mentioned earlier; that is, for 25° on both sides of Surveyor's longitude and for the latitude range going from 0° to ±12°. Without distinction of groups, the craters of this lunar area can be aligned according to the directions which are directly suggested by the lunar map. After this, lines of craters can be joined according

Example of the Distribution of the Lunar Craters
(I,II,III,...,VI, groups of Fig. 10)

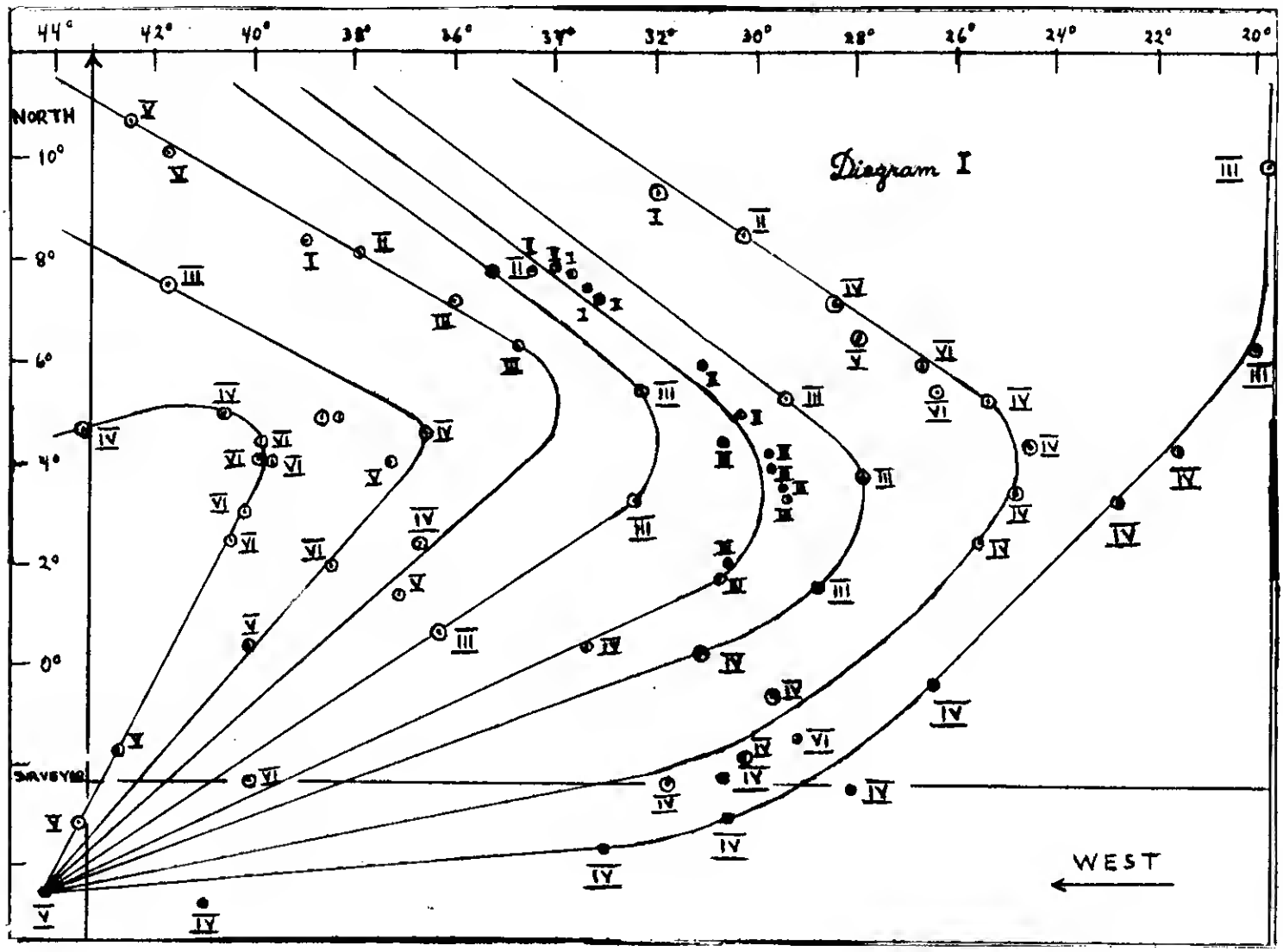

to their respective convergences, the final convergence being marked by the alignment of small craters. Finally, identification of the different groups of craters in Figure 10 can be made by using the difference in A_0 mentioned above.

An example of this procedure is shown in Diagram I for lunar surface analyzed between 20°W and 44°W and for latitudes going from -5° to +11°. (Although the selenographic coordinates of Surveyor are indicated in Diagram I, the difference in A_0 are referred, as indicated above, to the difference in A_0 corresponding to Flamsteed.)

For the lunar area of 25° on both sides of Surveyor's longitude and for the latitude range going from 0° to ±12°, the results of the analysis can be summarized as follows: (1) The curves shown in Diagram I also appear in the Western Hemisphere but they evolve in an opposite sense. (2) For all curves, the convergences seem to occur at about the latitude corresponding to the center of Oceanus Procellarum. On the Eastern Hemisphere, they are directed toward Copernicus but slightly modified in their path by the presence of Kepler. On the Western Hemisphere, they are directed toward Cavalerius and their path is also slightly modified by the presence of Reiner. (3) The extremes of curves end successively at craters which are approximately situated along the longitude that runs through the center of Oceanus Procellarum; the last curve, in each hemisphere of this center, has ends at Aristarchus, while the other extreme ends in the center of a triangle formed by Gassendi, Mersenius and Zupus. One may notice that convergences at Flamsteed shown in Diagram I are only a result of taking that crater as a reference point. Actually, the extremes always end on craters, situated in the longitude cited, and Flamsteed is located in this longitude.

For Oceanus Procellarum, lunar craters do not show any meteorite impact origin, as is claimed by many authors.

Their evolution, which will be discussed soon, also does not indicate subsequent modification by impacts of meteorites. From the finding of two families with their corresponding groups of craters, the following is apparent: (1) The origin of lunar craters seems due to internal and almost superficial explosions. The family composed of groups I, II and III is due to the first type of explosion. Because the inner material is more or less ejected on the lunar surface, these groups of craters often have rays which consist of material that reflects more sunlight than it absorbs. The family composed of groups IV, V and VI is due to the second type of explosion; the material ejected, not too far from the crater's center, comes from a relatively small depth and this is the reason that such craters are not rayed and, therefore, adsorb more sunlight than they reflect. (2) If explosions are small but numerous in a very thick layer, then the resulting "bubbling effect" would form a tremendous quantity of "minute, very small and smaller" craters on the lunar surface. Since the moon is not a "dead body", a weak and almost superficial activity may cause coloration changes (brightening or darkening) on the surface; this would explain the two cases A_r and A_s previously described.

With regard to the evolution of craters, a graphical representation is given in Figure 19 for some examples of craters considered in Figure 14. The word "evolution" used here is not related to the age but to the way in which craters were formed with respect to the strength of material ejection and ejection angle with respect to the lunar surface. Judging from Figure 19, the size does not necessarily correspond

to the sequence groups I, II and III or IV, V and VI in the families shown. The impression is that, for the family of groups I, II and III, such evolution has been as follows: (1) If the strength of ejection material is strong and the said material has been ejected at an angle nearly normal to the lunar surface, the resulting crater is both large and has large extensions of material radiating from its rims; examples are Copernicus, Kepler and Aristarchus. (2) If the strength of ejection material is strong but the angle is less important than that of (1), the crater would always be large, but not have such extensive rays; this is the case of the crater Euler. (3) If the strength of ejection material is moderate and the ejection occurs at medium angle, the resulting crater would not be as large and its rays would not go far from the rims; Kepler C is a good example. In relation to the family of groups IV, V and VI, the explanation above would be the same with the difference being that the ejected material comes from a relatively shallow depth.

CONCLUSION

In conclusion, the "equivalent albedo" obtained in this third report indicates that the astronaut should not explore certain types of craters. It is difficult to say in what way his life might be exposed to dangers, but, from this analysis, it appears that the groups I, II and III of craters are not completely extinguished as yet. Also, the smaller craters designated by A_r and A_s must be avoided since they seem to be a sign of some weak, but almost constant, lunar activity fairly close to the surface. This is also indicated in Figure 20, where groups of the first family show a decreasing "equivalent albedo" from the periphery in toward the center. Also, with respect to the cases A_r and A_s, one sees in Figure 21 that they are just between the two families of craters already mentioned. Identification of rayed craters, including A_r and A_s craters prior to the launch of the manned spacecraft, can be made by using the procedure explained in Figure 15.

PROGRAM RECOMMENDED TO ASSIST THE NASA LUNAR APOLLO PROGRAM

As related in the preceding Reports 1 and 2, and also described in this report, the aim of this research is to assist NASA in its efforts to select the safest area for landing a manned spacecraft on the lunar surface. The fact that it is a question of a manned spacecraft has made it necessary to attempt to obtain the most precise analysis possible of lunar photographs before preparing final recommendations on this subject. Hence, the rationale for a precise method of data reduction, to analyze the behavior of lunar temperature, the lunar morphology, peculiarities of specific surface topographic features and, finally, to determine as much as possible about the composition of the potential landing sites was developed. After the conception of the method for extrapolating data by using the successive transformations, and its direct application to the study of lunar temperature and surface composition, lunar photography analyses will be completed with specific spectral photometric and polarimetric interpretations for interesting lunar landing sites.

To assist the Nasa Lunar Apollo Program, the "Successive Transformation Method" has been applied to the study of Ranger, Surveyor and Orbiter photographs following the pattern shown below:

First Part: (I) - General development of the new data extrapolation method (completed). (II) - First application to study the variation of behavior of the lunar surface temperature (completed). (III) -

Second application to the study of the composition of the lunar material (completed). IV) - Addendum: Test of the data extrapolation method procedure by localizing Surveyor on the lunar surface and, also, by showing that an Orbiter II photograph attributed to Copernicus corresponds to Kepler.

Second Part: (V) - Analysis of the Ranger, Surveyor and Orbiter photographs using the results obtained from steps (II) and (III). (VI) - Detailed study of the selected landing sites of NASA utilizing the results obtained from steps (II), (III) and (V). (VII) - Using the results obtained from steps (II), (III), (V) and (VI), preparation of recommendations for the landing of the spacecraft and for the astronaut. (VIII) - Addendum: To obtain additional information such as using lunar spectral photometric and polarimetric observations in order to perfect the recommendations furnished by step (VII).

ACKNOWLEDGMENTS

The completion of the First Part of this report series has been possible with the collaboration of Mr. Keith Westhusing, from the Lockheed Electronics Company, Section of the Geophysical Laboratory, who kindly reviewed and made the necessary corrections of Reports I, II and III. Also, Mr. Roland R. Vela, from the Mapping Science Department, has permitted the use of his technique for utilizing lunar temperature contours as has been discussed in Report II. Other persons have contributed time and effort to this research which applies the "Successive Transformations Method" to lunar landing problems. These persons are: Kenneth Renfro, D. Spooner, Frank Wilhite, Bruce Kates, and William Barker; the first two people are attached to the Mapping Science Department and the last named are assigned to the Geophysical Laboratory of which William Barker is the overall manager. Finally, gratefulness must be expressed to Rollie Woodruff, Director, and to Dr. Jackson Barnes, Supervisor, and to all of my colleagues, Mrs. Elizabeth Dillinger, Dr. Luis Flores, Dr. B. S. Carroll, and Dr. M. Meicler, of the Analysis Department of Lockheed Electronics Company, who assisted in the completion of Report III.

The writer is deeply indebted to all.

Appendix A

ILLUSTRATIONS

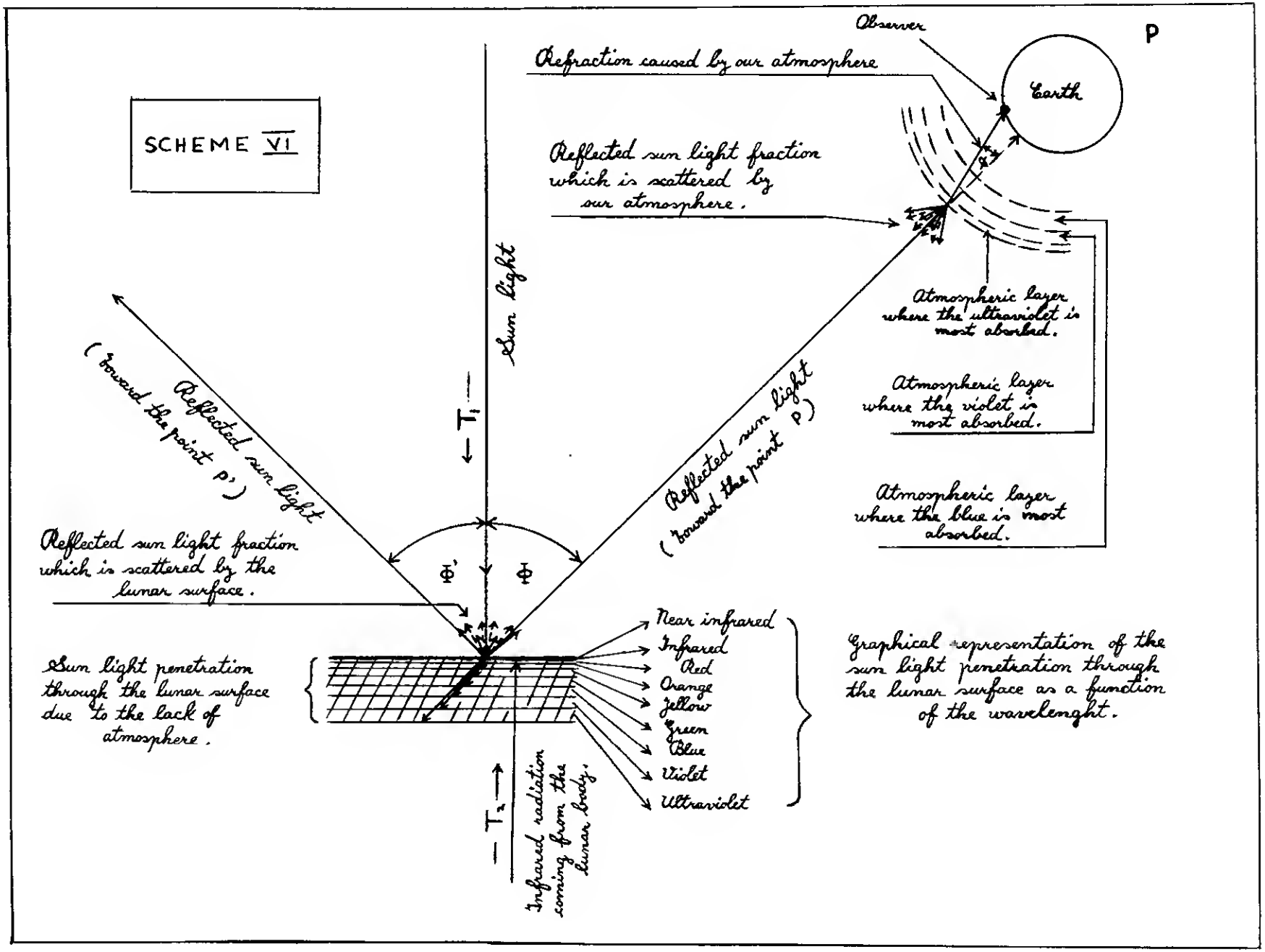
SCHEME VI
Observer
P
Earth
Refraction caused by our atmosphere
Reflected sun light fraction which is scattered by our atmosphere.
Sun light
T_1
Atmospheric layer where the ultraviolet is most absorbed.
Atmospheric layer where the violet is most absorbed.
Atmospheric layer where the blue is most absorbed.
Reflected sun light (toward the point P')
Reflected sun light (toward the point P)
Reflected sun light fraction which is scattered by the lunar surface.
Φ'
Φ
Sun light penetration through the lunar surface due to the lack of atmosphere.
Near infrared
Infrared
Red
Orange
Yellow
Green
Blue
Violet
Ultraviolet
Graphical representation of the sun light penetration through the lunar surface as a function of the wavelenght.
T_2
Infrared radiation coming from the lunar body.

VII a

Arbitrary definition of the Moon crater size.

∘ ⟶	minute crater	≈ 0.2	miles	in diameter
∘ ⟶	very small crater	≈ 0.4	»	» »
∘ ⟶	smaller crater	≈ 0.8	»	» »
∘ ⟶	small crater	≈ 1.2	»	» »
○ ⟶	medium size crater	≈ 2.0	»	» »
○ ⟶	large crater	≈ 5.6	»	» »
◯ ⟶	larger crater	≈ 7.0	»	» »

Largest ⟶ like the crater KEPLER or biger than this-one.

VII b

Direction adopted to read the effective temperatures.

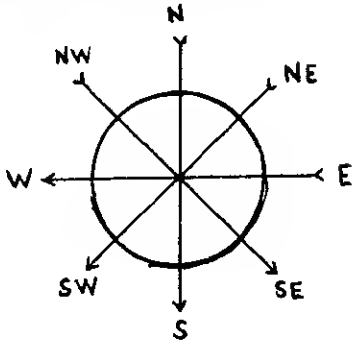

(Readings made from minute to large craters)

VII c

Procedure adopted to read the effective temperatures in the case of relatively flat surface, elevations and big craters.

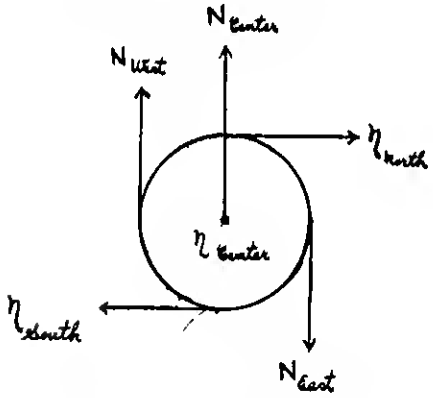

Relatively flat surface.

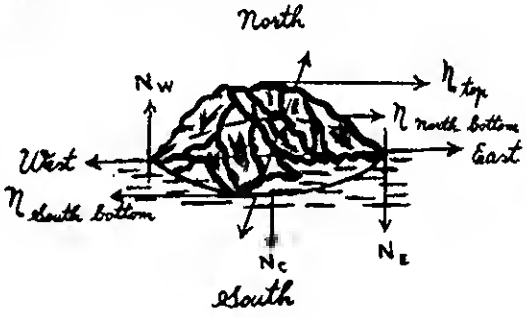

Elevation

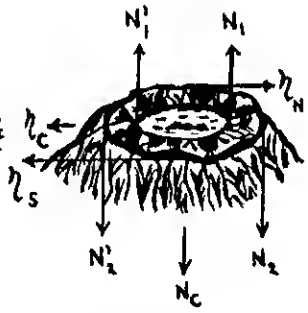

Depressions of larger and largest craters

VII d

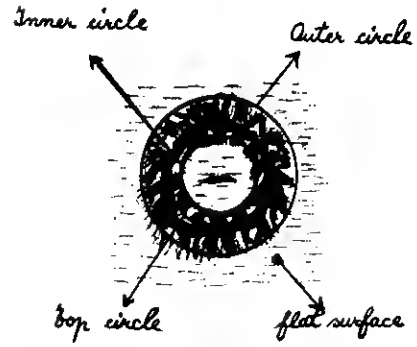

Non-extended rims crater.

SCHEME VII

VII e

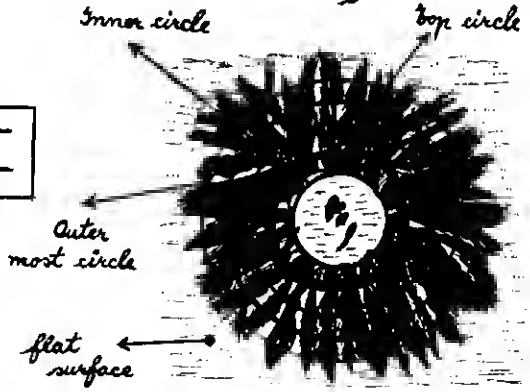

Extended rims crater

SCHEME VIII

Illumination at the lunar intensity equator

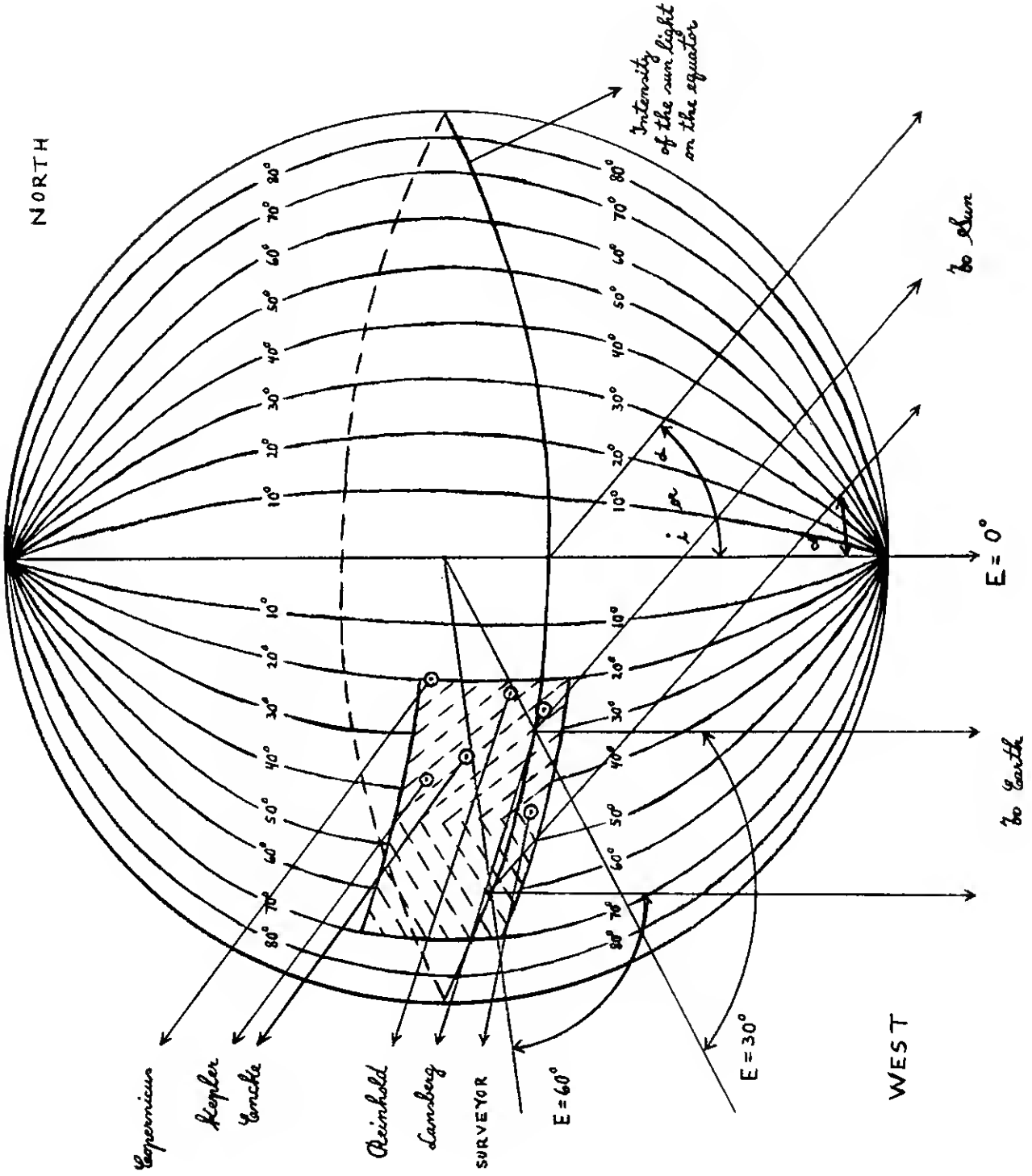

Procedure to avoid the Earth atmospheric absorption on the reflected sun light by the Moon.
P'
Sun
A, A', A" : Different positions of the Moon, in the same night, when observing a given lunar spot.
B : Reflected sun light fraction which is scattered by the lunar surface, (It is only graphically represented for the position A")
C and D : Scattering and refraction caused by our atmosphere.
Sun light to the Moon
Sun light to the Earth
Moon
Earth
Reflected sun light
(dark side)
Observer
P

SCHEME IX

TABLE 3

Equivalent albedos for craters determined from the effective temperatures given by SURVEYOR

Numerical order of crater	Size classification of crater	Coordinates: Longitude	Coordinates: Latitude	The slope η/N	Temperature ratio of crater	$\frac{N}{\eta}\delta\hat{T}_0$	Range of equivalent albedo
1	Very small	42°29'W	2°10'S	0.040	0.008	0.200	0.050
2	Very small	42°50'W	1°42'S	0.060	0.002	0.033	0.303
3	minute	42°18'W	1°15'S	0.034	0.015	0.441	0.022
4	Very small	42°28'W	0°33'S	0.037	0.002	0.054	0.185
5	Very small	42°59'W	0°47'N	0.098	0.010	0.102	0.098
6	Very small	43°15'W	0°53'N	0.098	0.010	0.102	0.098
7	minute	43°07'W	1°02'N	0.098	0.012	0.122	0.082
8	Very small	43°17'W	1°33'N	0.098	0.012	0.122	0.082
9	minute	43°08'W	2°00'N	0.098	0.015	0.153	0.065
10	minute	42°53'W	2°22'N	0.098	0.012	0.122	0.082
11	minute	42°09'W	2°00'N	0.053	0.005	0.094	0.106
12	minute	42°27'W	2°32'N	0.073	0.010	0.137	0.072
13	minute	42°05'W	4°18'N	0.064	0.005	0.078	0.128
14	Very small	43°10'W	7°08'N	0.098	0.015	0.160	0.062
15	Smaller	42°28'W	7°10'N	0.098	0.010	0.102	0.098
16	Medium	42°54'W	7°30'N	0.098	0.045	0.153	0.065
17	Minute	41°28'W	2°01'S	0.018	0.005	0.277	0.036
(18)	Minute	40°59'W	2°06'S	0.013	0.025	0.019	(0.019)
19	Small	40°32'W	2°20'S	0.014	0.005	0.357	0.028
(20)	Small	40°09'W	2°18'S	0.012	0.020	0.016	(0.016)
21	Minute	40°40'W	1°15'S	0.019	0.005	0.263	0.038
22	Minute	40°23'W	0°52'S	0.019	0.011	0.578	0.017
23	Medium	40°10'W	0°25'N	0.027	0.002	0.074	0.135
24	Smaller	41°15'W	0°56'N	0.023	0.002	0.087	0.114
25	Small	40°34'W	2°25'N	0.030	0.020	0.666	0.015
(26)	Very small	41°16'W	2°42'N	0.036	0.040	0.011	(0.011)
27	Small	40°57'W	3°17'N	0.033	0.018	0.545	0.018
28	Small	40°45'W	3°45'N	0.041	0.010	0.244	0.041
29	Small	40°42'W	4°12'N	0.039	0.008	0.205	0.049
30	Small	40°48'W	4°33'N	0.040	0.020	0.500	0.020
31	Medium	40°40'W	4°55'N	0.040	0.010	0.250	0.040
32	Large	41°47'W	7°27'N	0.066	0.005	0.075	0.133
(33)	Small	39°54'W	1°35'S	0.013	0.020	0.015	(0.015)
34	Minute	39°06'W	2°07'S	0.016	0.005	0.312	0.032
35	Minute	38°13'W	1°53'S	0.014	0.005	0.357	0.028
36	Minute	39°51'W	0°43'S	0.019	0.002	0.105	0.095
37	Very small	38°42'W	0°03'S	0.021	0.003	0.143	0.070
38	Very small	39°46'W	0°50'N	0.023	0.008	0.347	0.029
39	Very small	39°46'W	0°31'N	0.021	0.002	0.095	0.105
40	Very small	39°25'W	0°15'N	0.019	0.005	0.263	0.038
41	Smaller	39°04'W	0°12'N	0.017	0.008	0.470	0.021
42	Very small	38°23'W	0°21'N	0.019	0.007	0.368	0.027
43	Smaller	38°43'W	1°04'N	0.022	0.015	0.682	0.015
44	Minute	39°00'W	1°32'N	0.025	0.002	0.080	0.125
45	Small	38°28'W	1°58'N	0.022	0.004	0.182	0.055
46	Very small	38°47'W	1°59'N	0.024	0.005	0.208	0.048
47	Very small	39°09'W	2°33'N	0.024	0.005	0.208	0.048
48	Very small	39°21'W	2°40'N	0.025	0.002	0.080	0.125
49	Very small	39°27'W	3°18'N	0.026	0.008	0.307	0.032
50	Smaller	39°13'W	3°38'N	0.025	0.002	0.080	0.125
51	Smaller	38°07'W	3°49'N	0.025	0.006	0.240	0.042
52	Small	38°51'W	4°33'N	0.026	0.005	0.192	0.052

MAESTLIN →

KEPLER B →

TABLE 3 (continued)

Equivalent albedo for craters determined from the effective temperatures given by SURVEYOR

Numerical order of crater	Descriptive classification of crater	Coordinates: Longitude	Coordinates: Latitude	The slope η / N	Temperature variation of crater	$\frac{N}{\eta}\delta\hat{T}_0$	Range of equivalent albedo	
53	Medium	38°42'W	4°48'N	0.023	0.015	0.652	0.015	ENCKE D
54	Small	39°32'W	5°16'N	0.032	0.020	0.625	0.016	ENCKE J
55	Medium	38°27'W	7°25'N	0.034	0.010	0.294	0.034	
56	Small	39°25'W	7°48'N	0.036	0.020	0.555	0.018	
57	Medium	39°00'W	8°22'N	0.035	0.002	0.057	0.175	KEPLER C
58	Large	36°23'W	0°35'N	0.016	0.002	0.125	0.080	ENCKE C
59	Small	37°12'W	1°22'N	0.019	0.002	0.105	0.095	
60	Larger	36°43'W	2°20'N	0.020	0.005	0.250	0.040	ENCKE B
61	Smaller	37°38'W	1°53'N	0.021	0.002	0.095	0.105	
62	Smaller	37°43'W	2°30'N	0.022	0.002	0.091	0.190	
63	Small	36°34'W	2°52'N	0.020	0.002	0.100	0.100	
64	Small	37°22'W	4°00'N	0.023	0.002	0.066	0.151	
65	Largest	36°33'W	4°33'N	0.023	0.010	0.434	0.023	ENCKE
66	Small	36°21'W	5°52'N	0.024	0.002	0.083	0.120	
67	Small	36°30'W	6°03'N	0.025	0.002	0.080	0.125	
68	Larger	36°05'W	7°08'N	0.026	0.010	0.384	0.026	KEPLER A_0
69	Small	37°48'W	6°19'N	0.028	0.005	0.178	0.056	
70	Small	37°24'W	7°35'N	0.030	0.002	0.066	0.151	
71	Largest	38°00'W	8°00'N	0.032	0.002	0.063	0.158	KEPLER
72	Minute	34°03'W	2°08'S	0.013	0.002	0.153	0.065	
73	Minute	34°12'W	2°02'S	0.013	0.002	0.153	0.065	
74	Minute	34°48'W	1°23'S	0.013	0.002	0.153	0.065	
75	Minute	35°47'W	1°31'S	0.015	0.002	0.133	0.075	
76	Minute	35°28'W	1°28'S	0.014	0.002	0.142	0.070	
77	Minute	34°46'W	1°03'S	0.015	0.002	0.133	0.075	KEPLER A
78	Minute	35°48'W	0°59'S	0.016	0.002	0.125	0.080	KEPLER B
79	Minute	34°42'W	0°43'S	0.015	0.002	0.133	0.075	
80	Minute	34°20'W	0°38'S	0.015	0.002	0.133	0.075	
81	Minute	34°40'W	0°17'S	0.015	0.002	0.133	0.075	
82	Minute	35°37'W	0°10'S	0.017	0.002	0.117	0.085	
83	Minute	34°42'W	0°12'N	0.016	0.002	0.125	0.080	
84	Minute	34°59'W	2°37'N	0.020	0.002	0.100	0.100	
85	Minute	34°28'W	2°53'N	0.019	0.002	0.105	0.095	
86	Smaller	35°41'W	3°15'N	0.021	0.002	0.095	0.105	
87	Very small	35°42'W	3°33'N	0.022	0.002	0.091	0.190	
88	Smaller	35°15'W	4°28'N	0.022	0.002	0.091	0.190	
89	Smaller	35°05'W	4°27'N	0.021	0.002	0.095	0.105	
90	Small	35°10'W	5°15'N	0.022	0.002	0.091	0.190	
91	Minute	34°22'W	5°14'N	0.022	0.002	0.091	0.190	
92	Very small	34°44'W	5°34'N	0.022	0.002	0.091	0.190	
93	Very small	34°17'W	5°42'N	0.022	0.002	0.091	0.190	
94	Very small	35°53'W	5°27'N	0.025	0.002	0.080	0.125	
95	Smaller	35°32'W	5°47'N	0.024	0.002	0.083	0.120	
96	Smaller	34°53'W	5°58'N	0.024	0.002	0.083	0.120	
97	Small	34°52'W	6°03'N	0.023	0.002	0.066	0.151	
98	Smaller	34°50'W	6°18'N	0.023	0.002	0.066	0.151	
99	Small	35°56'N	6°28'N	0.026	0.002	0.076	0.131	
100	Very small	35°56'N	6°37'N	0.027	0.002	0.074	0.135	
101	Very small	35°19'W	6°55'N	0.025	0.002	0.080	0.125	
102	Very small	35°48'W	7°05'N	0.026	0.002	0.076	0.131	
103	Larger	36°09'W	7°08'N	0.028	0.010	0.357	0.028	
104	Large	35°18'W	7°35'N	0.026	0.005	0.192	0.052	

TABLE 3 (continued)

Equivalent albedos for craters determined from the effective temperatures given by SURVEYOR

Numerical order of crater	Size classification of crater	Coordinates: Longitude	Coordinates: Latitude	The slope η/N	Temperature vertex of crater	$N/\eta \, \delta \hat{T}_0$	Range of equivalent albedo	
105	Medium	35°05'W	7°53'N	0.025	0.002	0.080	0.125	
106	Minute	34°38'W	7°44'N	0.025	0.002	0.125	0.125	
107	Smaller	34°29'W	7°44'N	0.024	0.002	0.083	0.120	
108	Very small	33°50'W	2°12'S	0.013	0.002	0.153	0.065	
(109)	Minute	32°52'W	2°06'S	0.013	0.015	0.012	(0.012)	
(110)	Small	32°18'W	1°52'S	0.013	0.015	0.012	(0.012)	
111	Very small	32°13'W	1°28'S	0.013	0.002	0.153	0.065	
112	Small	32°53'W	1°22'S	0.013	0.002	0.153	0.065	
113	Small	33°58'W	1°14'S	0.015	0.005	0.333	0.030	
(114)	Very small	33°55'W	0°51'S	0.010	0.010	0.010	(0.010)	
115	Small	32°17'W	0°33'S	0.013	0.006	0.461	0.021	KUNOWSKY C₀ ←
116	Medium	32°20'W	0°13'S	0.014	0.005	0.357	0.028	KUNOWSKY C ←
117	Minute	32°10'W	0°06'S	0.013	0.002	0.153	0.065	
118	Minute	32°30'W	0°17'N	0.015	0.006	0.400	0.025	
119	Very small	33°23'W	0°17'N	0.016	0.005	0.312	0.032	LANSBERG F →
120	Very small	32°07'W	1°43'N	0.016	0.004	0.250	0.040	LANSBERG K →
121	Minute	32°13'W	2°45'N	0.017	0.002	0.117	0.085	LANSBERG A →
122	Larger	32°29'W	3°15'N	0.019	0.003	0.158	0.063	KUNOWSKY ←
123	Very small	32°56'W	3°41'N	0.019	0.002	0.105	0.095	
124	Very small	33°02'W	3°48'N	0.019	0.005	0.266	0.037	
125	Minute	33°39'W	4°00'N	0.019	0.007	0.368	0.027	
126	Minute	33°43'W	4°30'N	0.019	0.005	0.266	0.037	
127	Minute	33°48'W	4°40'N	0.021	0.002	0.095	0.105	
128	Minute	33°48'W	4°55'N	0.022	0.008	0.363	0.027	
129	Very small	32°52'W	5°05'N	0.020	0.005	0.250	0.040	
130	Large	32°18'W	5°23'N	0.020	0.002	0.100	0.100	HORTENSIUS 8 ←
131	Minute	32°28'W	5°33'N	0.021	0.002	0.095	0.105	
132	Medium	32°07'W	5°42'N	0.020	0.002	0.100	0.100	
133	Smaller	32°48'W	5°46'N	0.021	0.002	0.095	0.105	
134	Very small	32°58'W	6°18'N	0.022	0.005	0.227	0.044	
135	Very small	33°08'W	6°20'N	0.022	0.002	0.091	0.190	
136	Very small	32°57'W	6°28'N	0.022	0.005	0.227	0.044	
137	Small	33°11'W	7°11'N	0.024	0.010	0.416	0.024	
138	Small	33°25'W	7°22'N	0.023	0.002	0.066	0.151	
139	Very small	33°12'W	7°34'N	0.023	0.002	0.066	0.151	
140	Small	33°41'W	7°42'N	0.024	0.002	0.083	0.120	
141	Smaller	33°19'W	7°45'N	0.023	0.002	0.066	0.151	
142	Small	31°48'W	2°23'S	0.013	0.005	0.384	0.026	
143	Smaller	31°43'W	2°22'S	0.013	0.005	0.384	0.026	
144	Smaller	31°00'W	2°18'S	0.012	0.005	0.416	0.024	
145	Larger	30°38'W	2°13'S	0.012	0.015	0.416	0.024	
146	Medium	30°17'W	1°50'S	0.013	0.002	0.153	0.065	
147	Large	31°07'W	0°12'N	0.016	0.004	0.250	0.040	
148	Small	30°40'W	0°09'N	0.015	0.003	0.200	0.050	LANSBERG A₃₀ ←
149	Minute	31°43'W	0°47'N	0.017	0.002	0.117	0.085	
150	Minute	30°06'W	0°51'N	0.016	0.002	0.125	0.080	
151	Very small	30°23'W	0°59'N	0.016	0.002	0.125	0.080	
152	Minute	30°49'W	1°27'N	0.015	0.002	0.133	0.075	
153	Minute	30°19'W	1°25'N	0.016	0.002	0.125	0.080	
154	Minute	31°28'W	1°46'N	0.017	0.002	0.117	0.085	
155	Small	30°44'W	1°40'N	0.015	0.002	0.133	0.075	
156	Very small	30°20'W	1°43'N	0.017	0.005	0.292	0.034	

TABLE 3 (continued)

Equivalent albedo for craters determined from the effective temperatures given by SURVEYOR

Numerical order of crater	Size classification of crater	Coordinates: Longitude	Coordinates: Latitude	The slope η / N	Temperature vector of crater	$\frac{N}{\eta}\delta T_0$	Range of equivalent albedo		Numerical order of crater	Size classification of crater	Coordinates: Longitude	Coordinates: Latitude	The slope η / N	Temperature vector of crater	$\frac{N}{\eta}\delta T_0$	Range of equivalent albedo
157	Minute	30°18'W	2°13'N	0.017	0.005	0.294	0.034		183	Very small	28°27'W	1°51'N	0.016	0.005	0.312	0.032
158	Very small	31°13'W	2°16'N	0.018	0.002	0.111	0.090		184	Small	28°42'W	2°07'N	0.016	0.007	0.437	0.022
159	Very small	30°44'W	2°37'N	0.017	0.006	0.352	0.028		185	Smaller	28°58'W	2°12'N	0.017	0.005	0.294	0.034
160	Very small	31°02'W	3°00'N	0.018	0.005	0.277	0.036		186	Smaller	29°23'W	3°15'N	0.017	0.002	0.117	0.085
161	Minute	30°33'W	3°18'N	0.017	0.005	0.294	0.034		187	Smaller	29°28'W	3°28'N	0.017	0.010	0.588	0.017
162	Minute	31°18'W	3°28'N	0.017	0.002	0.117	0.085		188	Smaller	29°40'W	3°55'N	0.018	0.005	0.277	0.036
163	Very small	31°33'W	4°38'N	0.019	0.002	0.105	0.095		189	Small	29°44'W	4°09'N	0.018	0.002	0.111	0.090
164	Very small	31°07'W	4°36'N	0.019	0.002	0.105	0.095		190	Small	29°12'W	4°33'N	0.017	0.002	0.117	0.085
165	Smaller	31°03'W	4°26'N	0.019	0.002	0.105	0.095		191	Small	28°44'W	4°42'N	0.018	0.002	0.111	0.090
166	Larger	30°41'W	4°23'N	0.018	0.005	0.277	0.036	HORTENSIUS A ←	192	Very small	29°18'W	5°08'N	0.018	0.002	0.111	0.090
167	Smaller	30°20'W	4°57'N	0.018	0.002	0.111	0.090	HORTENSIUS D →	193	Small	29°26'W	5°17'N	0.019	0.002	0.105	0.095
168	Small	31°05'W	5°52'N	0.020	0.005	0.250	0.040		194	Small	29°00'W	5°22'N	0.018	0.010	0.555	0.018
169	Minute	30°22'W	7°07'N	0.020	0.015	0.750	0.013		195	Small	29°49'W	5°34'N	0.019	0.008	0.421	0.023
170	Minute	30°42'W	7°20'N	0.020	0.015	0.750	0.013		196	Very small	29°39'W	6°00'N	0.019	0.002	0.105	0.095
171	Minute	31°55'W	7°46'N	0.020	0.005	0.250	0.040		197	Very small	28°40'W	6°19'N	0.019	0.002	0.105	0.095
172	Very small	31°58'W	7°56'N	0.020	0.002	0.100	0.100		198	Very small	28°55'W	6°12'N	0.019	0.002	0.105	0.095
(173)	Very small	29°40'W	2°00'S	0.014	0.015	0.011	(0.01)		199	Smaller	29°21'W	6°22'N	0.019	0.002	0.105	0.095
174	Larger	29°13'W	1°30'S	0.013	0.010	0.769	0.013	LANSBERG C ←	(200)	Very small	29°37'W	6°40'N	0.020	0.020	0.010	(0.010)
175	Large	28°05'W	2°30'S	0.013	0.005	0.384	0.026	LANSBERG B ←	201	Small	29°49'W	6°48'N	0.020	0.015	0.750	0.013
176	Large	29°25'W	0°42'S	0.015	0.002	0.133	0.075	LANSBERG R ←	(202)	Very small	29°56'W	6°54'N	0.020	0.020	0.010	(0.010)
177	Small	29°40'W	0°37'S	0.014	0.002	0.142	0.070		203	Small	28°25'W	7°07'N	0.021	0.002	0.095	0.105
178	Small	28°12'W	0°28'N	0.015	0.002	0.133	0.075		204	Very small	28°29'W	1°57'S	0.013	0.002	0.133	0.065
179	Small	28°10'W	0°38'N	0.015	0.002	0.133	0.075		205	Small	26°29'W	1°55'S	0.013	0.005	0.384	0.026
(180)	Smaller	29°55'W	1°12'N	0.014	0.015	0.011	(0.01)		206	Small	26°08'W	1°48'S	0.013	0.005	0.384	0.026
181	Very small	29°28'W	1°31'N	0.014	0.005	0.357	0.028		207	Small	26°42'W	1°19'S	0.014	0.002	0.142	0.070
182	Small	28°48'W	1°30'N	0.016	0.002	0.125	0.080	KUNOWSKY D ←	208	Smaller	27°43'W	0°54'S	0.013	0.005	0.384	0.026

LANSBERG C ←

TABLE 3 (continued)

Equivalent albedos for craters determined from the effective temperatures given by SURVEYOR

Numerical order of craters	Size classification of craters	Coordinates: Longitude	Coordinates: Latitude	The slope η/N	Temperature variation of craters $N\frac{\delta T_0}{\epsilon}$		Range of equivalent albedo	
209	Largest	26° 32'W	0° 25'S	0.015	0.005	0.333	0.030	LANSBERG
210	Smaller	27° 20'W	0° 13'N	0.015	0.002	0.133	0.076	LANSBERG m
211	Medium	27° 50'W	1° 09'N	0.015	0.015	0.010	0.010	LANSBERG λ
212	Small	26° 34'W	0° 45'N	0.011	0.010	0.009	0.009	
213	Very small	26° 11'W	1° 32'N	0.015	0.002	0.133	0.076	
214	Very small	26° 10'W	2° 02'N	0.015	0.007	0.466	0.021	
215	Very small	27° 20'W	2° 08'N	0.016	0.002	0.125	0.080	LANSBERG 24
216	Very small	27° 37'W	3° 42'N	0.016	0.002	0.125	0.080	
217	Very small	26° 25'W	4° 00'N	0.017	0.005	0.294	0.034	
218	Small	27° 54'W	3° 45'N	0.017	0.005	0.294	0.034	HORTENSIUS ν
219	Small	26° 58'W	4° 00'N	0.018	0.005	0.277	0.036	
220	Small	26° 48'W	4° 07'N	0.018	0.010	0.555	0.018	
221	Smaller	26° 31'W	4° 23'N	0.018	0.010	0.555	0.018	
222	Very small	26° 48'W	4° 30'N	0.018	0.010	0.555	0.018	
223	Smaller	27° 20'W	4° 32'N	0.018	0.010	0.555	0.018	
224	Medium	27° 09'W	4° 40'N	0.018	0.010	0.555	0.018	HORTENSIUS s
225	Medium	26° 30'W	4° 52'N	0.018	0.010	0.555	0.018	
226	Very small	27° 21'W	4° 55'N	0.018	0.010	0.555	0.018	
227	Smaller	27° 23'W	5° 12'N	0.018	0.010	0.555	0.018	
228	Medium	26° 39'W	5° 25'N	0.018	0.010	0.555	0.018	
229	Medium	26° 43'W	5° 30'N	0.018	0.010	0.555	0.018	
230	Large	26° 42'W	5° 58'N	0.019	0.015	0.789	0.013	HORTENSIUS O
231	Very small	27° 19'W	5° 58'N	0.018	0.010	0.555	0.018	
232	Very small	27° 25'W	6° 03'N	0.018	0.010	0.555	0.018	
233	Very small	26° 48'W	6° 18'N	0.018	0.005	0.277	0.036	
234	Larger	27° 58'W	6° 26'N	0.019	0.010	0.578	0.017	HORTENSIUS
235	Small	26° 31'W	6° 37'N	0.018	0.002	0.111	0.090	
236	Small	26° 51'W	6° 55'N	0.018	0.002	0.111	0.090	
237	Very small	27° 33'W	7° 22'N	0.019	0.002	0.105	0.096	
238	Small	26° 13'W	7° 24'N	0.019	0.002	0.105	0.096	
239	Very small	25° 51'W	1° 59'S	0.013	0.010	0.769	0.013	
240	Large	25° 19'W	2° 16'S	0.013	0.010	0.769	0.013	
241	Large	25° 13'W	2° 00'S	0.013	0.010	0.769	0.013	
242	Very small	25° 12'W	2° 20'S	0.013	0.002	0.154	0.065	
243	Large	25° 10'W	1° 53'S	0.013	0.002	0.154	0.065	
244	Medium	25° 12'W	1° 42'S	0.014	0.002	0.154	0.065	
245	Small	24° 23'W	1° 43'S	0.014	0.002	0.154	0.065	
246	Smaller	25° 39'W	1° 22'S	0.014	0.002	0.154	0.065	
247	Smaller	25° 12'W	1° 22'S	0.014	0.002	0.154	0.065	
248	Minute	24° 48'W	1° 18'S	0.014	0.002	0.154	0.065	
249	Smaller	24° 25'W	1° 00'S	0.014	0.002	0.154	0.065	
250	Very small	25° 07'W	0° 56'S	0.014	0.002	0.154	0.065	
251	Minute	25° 28'W	0° 58'S	0.014	0.005	0.357	0.028	
252	Small	25° 43'W	0° 40'S	0.014	0.007	0.500	0.020	
253	Very small	25° 27'W	0° 05'S	0.014	0.007	0.500	0.020	
254	Minute	24° 43'W	0° 13'S	0.014	0.007	0.500	0.020	
255	Minute	24° 52'W	0° 05'S	0.014	0.010	0.714	0.014	
256	Minute	25° 31'W	0° 25'N	0.014	0.010	0.714	0.014	
257	Small	25° 28'W	1° 01'N	0.014	0.002	0.143	0.070	
258	Smaller	24° 13'W	1° 08'N	0.014	0.005	0.387	0.026	
259	Small	24° 13'W	1° 22'N	0.015	0.010	0.666	0.015	
260	Medium	25° 20'W	1° 32'N	0.015	0.010	0.666	0.015	REINHOLD 24

TABLE 3 (continued)

Equivalent albedos for craters determined from the effective temperatures given by SURVEYOR

Numerical order of crater	Size classification of craters	Coordinates Longitude	Coordinates Latitude	the slope η/N	temperature vertex of craters	$\frac{N}{\eta}\delta\hat{T}_0$	Range of equivalent albedo	
261	Smaller	25°09'W	1°45'N	0.015	0.002	0.133	0.075	
262	Small	25°21'W	1°57'N	0.015	0.002	0.133	0.075	
263	Very small	24°20'W	1°33'N	0.015	0.002	0.133	0.075	
264	Smaller	24°09'W	1°48'N	0.016	0.002	0.125	0.080	
265	Large	25°48'W	2°20'N	0.016	0.002	0.125	0.080	REINHOLD 8 ←
266	Small	25°34'W	2°27'N	0.016	0.002	0.125	0.080	
267	Very small	25°20'W	2°28'N	0.016	0.002	0.125	0.080	
268	Very small	24°59'W	2°27'N	0.016	0.005	0.312	0.032	
269	Small	24°33'W	2°31'N	0.016	0.005	0.312	0.032	
270	Small	25°18'W	2°57'N	0.016	0.002	0.125	0.080	
271	Small	24°18'W	3°12'N	0.016	0.002	0.125	0.080	
272	Very small	24°53'W	3°22'N	0.016	0.002	0.125	0.080	
273	Minute	25°29'W	3°24'N	0.016	0.002	0.125	0.080	
274	Small	24°30'W	4°19'N	0.017	0.002	0.118	0.084	REINHOLD 10 ←
275	Very small	24°22'W	4°25'N	0.017	0.002	0.118	0.084	
276	Small	25°37'W	4°41'N	0.017	0.005	0.294	0.034	
277	Minute	25°07'W	5°02'N	0.017	0.005	0.294	0.034	
278	Minute	24°38'W	5°02'N	0.017	0.010	0.588	0.017	
279	Larger	25°23'W	5°13'N	0.017	0.010	0.588	0.017	HORTENSIUS E ←
280	Minute	25°52'W	5°16'N	0.017	0.010	0.588	0.017	
281	Minute	24°45'W	5°16'N	0.017	0.010	0.588	0.017	
282	Minute	24°33'W	5°29'N	0.017	0.010	0.588	0.017	REINHOLD 1 →
283	Minute	24°42'W	5°43'N	0.017	0.010	0.588	0.017	
284	Medium	24°38'W	5°41'N	0.017	0.010	0.588	0.017	
285	Very small	24°04'W	6°10'N	0.018	0.010	0.555	0.018	
286	Medium	24°28'W	6°05'N	0.018	0.010	0.555	0.018	
287	Very small	25°08'W	6°13'N	0.018	0.010	0.555	0.018	
288	Minute	24°23'W	6°18'N	0.018	0.005	0.555	0.018	
289	Small	25°26'W	6°43'N	0.018	0.010	0.555	0.018	
290	Small	24°13'W	6°39'N	0.018	0.005	0.555	0.018	
291	Medium	25°25'W	6°55'N	0.018	0.010	0.555	0.018	HORTENSIUS 4 ←
292	Very small	24°17'W	7°08'N	0.018	0.010	0.555	0.018	
293	Very small	24°20'W	7°22'N	0.018	0.010	0.555	0.018	
294	Very small	24°27'W	7°25'N	0.018	0.010	0.555	0.018	
295	Very small	24°30'W	7°23'N	0.018	0.010	0.555	0.018	
296	Medium	25°43'W	7°28'N	0.018	0.010	0.555	0.018	
297	Medium	25°18'W	7°49'N	0.018	0.010	0.555	0.018	
298	Medium	25°11'W	7°48'N	0.018	0.010	0.555	0.018	
299	Minute	24°17'W	7°08'N	0.018	0.010	0.555	0.018	
300	Very small	22°59'W	2°25'S	0.013	0.002	0.154	0.064	
301	Smaller	23°29'W	1°57'S	0.013	0.002	0.154	0.064	
302	Smaller	23°54'W	1°37'S	0.014	0.002	0.143	0.070	
303	Minute	23°54'W	1°27'S	0.014	0.007	0.500	0.020	
304	Minute	23°48'W	0°50'S	0.014	0.009	0.644	0.016	
305	Smaller	22°53'W	0°39'S	0.014	0.006	0.429	0.024	
306	Smaller	22°52'W	0°30'S	0.014	0.008	0.571	0.018	
(307)	Very small	23°41'W	0°25'S	0.015	0.015	0.000	0.000	
308	Small	22°20'W	0°03'N	0.015	0.004	0.266	0.038	
309	Minute	23°19'W	0°11'N	0.015	0.003	0.200	0.050	
(310)	Minute	23°22'W	0°31'N	0.015	0.015	0.000	0.000	
311	Very small	23°22'W	0°49'N	0.015	0.003	0.200	0.050	
312	Minute	23°53'W	0°47'N	0.015	0.010	0.666	0.015	

TABLE 3 (continued)

Equivalent albedo for craters determined from the effective temperatures given by SURVEYOR

Numerical order of craters	Size classification of craters	Coordinates: Longitude	Coordinates: Latitude	the slope η/N	temperature variation of craters	$\frac{N}{\eta}\delta T_0$	Range of equivalent albedo	
313	Smaller	22°53'W	1°00'N	0.015	0.010	0.666	0.015	
314	Small	23°19'W	1°12'N	0.015	0.005	0.333	0.030	
315	Minute	22°52'W	1°19'N	0.015	0.005	0.333	0.030	
316	Minute	23°19'W	1°31'N	0.015	0.005	0.333	0.030	
317	Small	23°51'W	1°49'N	0.015	0.005	0.333	0.030	
318	Minute	23°11'W	1°50'N	0.015	0.005	0.333	0.030	
319	Small	22°45'W	1°59'N	0.015	0.005	0.333	0.030	
320	Small	22°19'W	2°13'N	0.015	0.005	0.333	0.030	
321	Very small	23°18'W	2°11'N	0.015	0.005	0.333	0.030	
322	Minute	23°16'W	2°22'N	0.015	0.005	0.333	0.030	COPERNICUS 27 →
323	Minute	23°52'W	2°39'N	0.015	0.010	0.666	0.015	
324	Very small	23°37'W	2°58'N	0.015	0.010	0.666	0.015	
325	Minute	23°37'W	3°08'N	0.015	0.010	0.666	0.015	COPERNICUS N →
326	Very small	23°41'W	3°30'N	0.015	0.010	0.666	0.015	
327	Largest	22°49'W	3°12'N	0.016	0.010	0.625	0.016	← REINHOLD
328	Smaller	22°03'W	3°52'N	0.016	0.010	0.625	0.016	
329	Smaller	22°09'W	3°59'N	0.016	0.010	0.625	0.016	COPERNICUS 20 →
330	Smaller	22°39'W	4°32'N	0.016	0.010	0.625	0.016	
331	Smaller	22°46'W	4°49'N	0.016	0.005	0.313	0.032	
332	Minute	23°46'W	4°37'N	0.016	0.005	0.313	0.032	
333	Minute	23°29'W	5°07'N	0.016	0.005	0.313	0.032	
334	Very small	23°29'W	5°32'N	0.016	0.005	0.313	0.032	
335	Very small	23°09'W	5°18'N	0.016	0.005	0.313	0.032	← REINHOLD t
336	Very small	22°56'W	5°30'N	0.016	0.010	0.666	0.015	
337	Very small	22°18'W	5°45'N	0.016	0.010	0.666	0.015	
338	Smaller	22°37'W	5°47'N	0.016	0.010	0.666	0.015	
339	Smaller	22°08'W	5°58'N	0.016	0.010	0.666	0.015	
340	Minute	23°39'W	5°25'N	0.016	0.015	0.009 0.009	0.009	
341	Small	23°51'W	6°06'N	0.017	0.015	0.009 0.009	0.009	
342	Smaller	23°43'W	6°20'N	0.017	0.010	0.588	0.017	
343	Minute	23°15'W	6°00'N	0.017	0.005	0.294	0.034	
344	Minute	22°25'W	6°12'N	0.017	0.005	0.294	0.034	
345	Minute	23°00'W	6°12'N	0.017	0.005	0.294	0.034	
346	Minute	22°30'W	6°25'N	0.017	0.005	0.294	0.034	
347	Smaller	22°23'W	6°28'N	0.017	0.005	0.294	0.034	
348	Smaller	22°42'W	6°25'N	0.017	0.005	0.294	0.034	
349	Smaller	22°48'W	6°36'N	0.017	0.005	0.294	0.034	
350	Smaller	23°22'W	6°46'N	0.017	0.005	0.294	0.034	
351	Small	23°28'W	7°00'N	0.017	0.005	0.294	0.034	
352	Minute	23°18'W	7°10'N	0.017	0.005	0.294	0.034	
353	Minute	23°11'W	7°25'N	0.017	0.005	0.294	0.034	
354	Minute	23°11'W	7°28'N	0.017	0.005	0.294	0.034	
355	Small	23°39'W	7°36'N	0.017	0.004	0.235	0.043	
356	Small	23°18'W	7°48'N	0.017	0.004	0.235	0.043	
357	Minute	23°09'W	7°39'N	0.017	0.004	0.235	0.043	
358	Minute	22°18'W	7°30'N	0.017	0.003	0.176	0.056	
359	Small	22°10'W	7°36'N	0.017	0.003	0.176	0.056	
360	Small	22°07'W	7°58'N	0.017	0.003	0.176	0.056	
360a	Small	20°59'W	2°02'S	0.013	0.013	0.010	0.010	← FRA MAURO t
360b	Small	20°39'W	1°42'S	0.013	0.002	0.153	0.065	
360c	Smaller	21°17'W	1°45'S	0.013	0.013	0.010	0.010	
360d	Smaller	20°23'W	1°08'S	0.013	0.002	0.153	0.065	

N.B. : the numbers 360a, 360b, 360c and 360d are just figures corresponding to craters forgotten before to take the number 361.

TABLE 3 (continued)

Equivalent albedo for craters determined from the effective temperatures given by SURVEYOR

Numerical order of crater	Size classification of crater	Coordinates: Longitude	Coordinates: Latitude	Temperature ratio of craters	The slope η / N	$\frac{N}{\eta} \delta T_0$	Range of equivalent albedo	
361	Very small	20°36'W	1°00'S	0.013	0.002	0.153	0.065	
362	Small	20°49'W	0°48'S	0.013	0.010	0.769	0.013	
363	Smaller	20°48'W	0°33'S	0.013	0.010	0.769	0.013	FAUTH →
364	Smaller	21°40'W	0°41'S	0.013	0.010	0.769	0.013	
365	Small	21°51'W	0°29'S	0.013	0.010	0.769	0.013	
366	Medium	21°03'W	0°14'S	0.013	0.010	0.769	0.013	REINHOLD K ←
367	Medium	21°43'W	0°10'N	0.013	0.002	0.153	0.065	
368	Small	~~20°18'W~~ 21°33'W	0°16'N	0.014	0.002	0.142	0.070	
369	Small	20°18'W	0°52'N	0.014	0.005	0.357	0.028	GAMBART AS ←
370	Minute	20°38'W	0°52'N	0.014	0.005	0.357	0.028	
371	Small	22°00'W	1°09'N	0.014	0.005	0.357	0.028	
372	Very small	21°42'W	1°15'N	0.014	0.007	0.500	0.020	
373	Smaller	21°12'W	1°39'N	0.014	0.007	0.500	0.020	
374	Very small	21°29'W	2°12'N	0.014	0.007	0.500	0.020	
375	Small	20°18'W	2°28'N	0.014	0.005	0.357	0.028	GAMBART AC ←
376	Smaller	20°48'W	2°42'N	0.014	0.004	0.285	0.035	
377	Medium	21°24'W	3°25'N	0.014	0.004	0.285	0.035	
378	Small	20°08'W	3°45'N	0.015	0.002	0.133	0.075	
379	Medium	20°39'W	4°07'W	0.015	0.010	0.666	0.015	REINHOLD N ←
380	Largest	21°38'W	4°15'N	0.015	0.005	0.333	0.030	REINHOLD A ←
381	Small	21°07'W	4°42'N	0.015	0.006	0.400	0.025	
382	Very small	20°11'W	4°55'N	0.015	0.006	0.400	0.025	
383	Small	20°49'W	5°19'N	0.015	0.006	0.400	0.025	
(384)	Minute	20°33'W	5°12'N	0.015	0.015	0.010	(0.010)	
385	Smaller	21°17'W	5°38'N	0.015	0.006	0.400	0.025	
(386)	Minute	21°06'W	5°39'N	0.015	0.015	0.010	(0.010)	COPERNICUS →

Numerical order of crater	Size classification of crater	Coordinates: Longitude	Coordinates: Latitude	The slope η / N	Temperature ratio of craters	$\frac{N}{\eta} \delta T_0$	Range of equivalent albedo
(387)	Very small	21°16'W	5°40'N	0.016	0.015	0.009	(0.009)
388	Very small	20°58'W	5°58'N	0.016	0.008	0.500	0.020
389	Larger	20°07'W	6°15'N	0.016	0.008	0.500	0.020
390	Very small	20°52'W	6°18'N	0.016	0.010	0.625	0.016
391	Smaller	21°32'W	6°04'N	0.016	0.010	0.625	0.016
392	Minute	21°22'W	6°25'N	0.016	0.010	0.625	0.016
393	Minute	21°17'W	6°28'N	0.016	0.010	0.625	0.016
394	Minute	21°19'W	7°05'N	0.016	0.010	0.625	0.016
395	Minute	21°19'W	7°08'N	0.017	0.005	0.294	0.034
396	Minute	21°12'W	7°45'N	0.017	0.005	0.294	0.034
397	Smaller	20°48'W	7°58'N	0.017	0.005	4294	0.034
398	Minute	20°49'W	7°11'N	0.017	0.005	0.294	0.034
399	Smaller	21°00'W	7°07'N	0.017	0.005	0.294	0.034
400	Smaller	21°08'W	7°03'N	0.017	0.007	0.412	0.024
401	Minute	21°13'W	7°01'N	0.017	0.007	0.412	0.024
402	Smaller	21°19'W	8°12'N	0.017	0.007	0.412	0.024
403	Minute	21°57'W	8°01'N	0.017	0.004	0.235	0.042
404	Minute	21°59'W	8°13'N	0.017	0.004	0.235	0.042
405	Minute	21°40'W	8°48'N	0.017	0.004	0.235	0.042
406	Minute	21°43'W	8°50'N	0.017	0.004	0.235	0.042
407	Minute	22°23'W	8°34'N	0.017	0.002	0.118	0.084
408	Smaller	22°48'W	9°11'W	0.018	0.002	0.111	0.090
409	Smaller	22°51'W	9°17'N	0.018	0.002	0.111	0.090
410	Smaller	22°16'W	9°14'N	0.018	0.002	0.111	0.090
411	Minute	21°53'W	9°07'N	0.018	0.002	0.111	0.090
412	Largest	20°00'W	9°40'N	0.018	0.002	0.111	0.090

TABLE 4

Equivalent albedo for elevations determined from the effective temperatures given by SURVEYOR

Numerical order of elevations	Coordinates		The slope η / N	Temperature of the elevation $\frac{N}{\eta}\delta T_0$		Range of equivalent albedo
	Longitude	Latitude				
1	43° 19' W	1° 40' S	0.095	0.020	0.210	0.047
2	43° 00' W	1° 43' S	0.033	0.010	0.303	0.033
3	43° 00' W	3° 25' S	0.048	0.013	0.270	0.037
4	43° 09' W	4° 00' S	0.085	0.018	0.212	0.047
5	42° 13' W	11° 00' S	0.099	0.023	0.232	0.043
6	42° 23' W	2° 48' S	0.024	0.007	0.292	0.038
7	42° 25' W	3° 45' S	0.034	0.008	0.235	0.042
8	42° 42' W	4° 30' S	0.047	0.013	0.277	0.036
9	42° 33' W	5° 38' S	0.059	0.005	0.084	0.119
10	42° 19' W	0° 05' N	0.043	0.007	0.163	0.061
11	42° 38' W	0° 45' N	0.053	0.009	0.170	0.059
12	42° 42' W	1° 22' N	0.066	0.018	0.273	0.036
13	42° 17' W	3° 48' N	0.076	0.020	0.263	0.038
14	42° 23' W	5° 00' N	0.091	0.020	0.220	0.045
15	40° 49' W	11° 37' S	0.052	0.030	0.576	0.017
16	40° 38' W	11° 11' S	0.049	0.033	0.673	0.015
17	40° 19' W	10° 35' S	0.044	0.034	0.773	0.013
18	40° 19' W	10° 09' S	0.040	0.030	0.750	0.013
19	41° 00' W	8° 42' S	0.038	0.020	0.689	0.014
20	40° 34' W	8° 00' S	0.037	0.020	0.541	0.018
21	40° 42' W	7° 32' S	0.036	0.020	0.555	0.018
22	40° 51' W	6° 42' S	0.035	0.020	0.571	0.018
23	40° 59' W	6° 00' S	0.035	0.004	0.114	0.088
24	41° 12' W	5° 27' S	0.034	0.013	0.382	0.034
25	41° 45' W	4° 47' S	0.034	0.017	0.500	0.200
26	40° 41' W	1° 23' N	0.028	0.022	0.785	0.130
27	40° 30' W	1° 43' N	0.027	0.022	0.814	0.012
28	40° 23' W	2° 00' N	0.029	0.022	0.758	0.013
29	40° 42' W	2° 38' N	0.030	0.020	0.666	0.015
30	40° 41' W	3° 05' N	0.030	0.019	0.633	0.015
31	40° 23' W	3° 20' N	0.033	0.026	0.787	0.013
32	40° 20' W	3° 43' N	0.035	0.024	0.685	0.015
33	40° 38' W	4° 08' N	0.036	0.028	0.787	0.013
34	41° 22' W	4° 19' N	0.050	0.028	0.560	0.017
35	41° 42' W	4° 33' N	0.061	0.031	0.518	0.019
36	41° 49' W	4° 55' N	0.063	0.033	0.524	0.019
37	Tycho	North rim	0.040	0.030	0.750	0.013
38	Tycho	~~South~~ NE rim	0.039	0.030	0.769	0.013
39	Tycho	East rim	0.038	0.030	0.789	0.013
40	Tycho	SE rim	0.036	0.028	0.777	0.013
41	Tycho	South rim	0.034	0.024	0.765	0.013
42	Tycho	SW rim	0.036	0.026	0.722	0.014
43	Tycho	West rim	0.037	0.029	0.784	0.013
44	Tycho	NW rim	0.039	0.029	0.744	0.013
45	Kepler	North rim	0.070	0.020	0.285	0.035
46	Kepler	NE rim	0.066	0.018	0.273	0.037
47	Kepler	East rim	0.062	0.015	0.242	0.041
48	Kepler	SE rim	0.065	0.018	0.277	0.036
49	Kepler	South rim	0.068	0.018	0.265	0.037
50	Kepler	SW rim	0.070	0.021	0.300	0.033
51	Kepler	West rim	0.072	0.024	0.333	0.030
52	Kepler	NW rim	0.071	0.022	0.308	0.025
53	40° 28' W	9° 33' N	0.048	0.020	0.416	0.024
54	40° 12' W	9° 45' N	0.044	0.018	0.409	0.024
55	38° 14' W	10° 57' S	0.028	0.006	0.214	0.045
56	38° 30' W	10° 39' S	0.028	0.006	0.214	0.045
57	38° 30' W	10° 17' S	0.027	0.005	0.185	0.054
58	38° 21' W	9° 50' S	0.026	0.004	0.154	0.064
59	38° 40' W	9° 23' S	0.026	0.004	0.154	0.064
60	38° 22' W	8° 45' S	0.025	0.004	0.160	0.063
61	39° 31' W	9° 26' S	0.028	0.004	0.143	0.070
62	39° 31' W	8° 35' S	0.030	0.004	0.133	0.075
63	39° 46' W	6° 19' S	0.024	0.004	0.166	0.060
64	39° 42' W	6° 00' S	0.023	0.004	0.174	0.057
65	39° 09' W	5° 41' S	0.022	0.004	0.182	0.055
66	38° 48' W	5° 41' S	0.021	0.004	0.190	0.053
67	38° 21' W	5° 41' S	0.020	0.004	0.200	0.050
68	39° 20' W	3° 28' S	0.015	0.010	0.666	0.015
69	39° 31' W	2° 51' S	0.014	0.010	0.714	0.014
70	39° 13' W	2° 11' N	0.022	0.006	0.273	0.037
71	39° 13' W	2° 20' N	0.023	0.006	0.260	0.038
72	39° 32' W	2° 37' N	0.024	0.006	0.250	0.040
73	39° 38' W	3° 07' N	0.025	0.006	0.240	0.042
74	39° 39' W	3° 22' N	0.026	0.006	0.231	0.043
75	39° 37' W	3° 48' N	0.027	0.006	0.222	0.045
76	39° 25' W	3° 57' N	0.028	0.006	0.214	0.047
77	39° 16' W	7° 11' N	0.038	0.003	0.078	0.126
78	38° 04' W	7° 30' N	0.038	0.003	0.078	0.126

TABLE 4 (continued)

Equivalent albedo for elevations determined from the effective temperatures given by SURVEYOR

Numerical order of elevations	Coordinates		The slope η/N	Temperature of the elevation	$\frac{N}{\eta}\delta T_0$	Range of equivalent albedo
	Longitude	Latitude				
79	36° 11' W	9° 54' S	0.023	0.018	0.769	0.013
80	36° 27' W	9° 38' S	0.022	0.017	0.772	0.013
81	36° 22' W	9° 19' S	0.021	0.016	0.761	0.013
82	36° 19' W	8° 48' S	0.021	0.016	0.761	0.013
83	37° 31' W	8° 45' S	0.024	0.004	0.166	0.060
84	37° 13' W	8° 09' S	0.022	0.004	0.166	0.060
85	37° 33' W	7° 55' S	0.022	0.004	0.166	0.060
86	37° 52' W	6° 35' S	0.020	0.004	0.200	0.050
87	37° 48' W	6° 11' S	0.019	0.004	0.200	0.050
88	37° 12' W	6° 00' S	0.019	0.004	0.200	0.050
89	37° 58' W	5° 12' S	0.018	0.004	0.200	0.050
90	36° 17' W	3° 00' S	0.013	0.033	0.393	0.025
91	36° 26' W	2° 25' S	0.013	0.033	0.393	0.025
92	36° 42' W	2° 11' S	0.014	0.033	0.393	0.025
93	36° 44' W	1° 42' S	0.014	0.033	0.393	0.025
94	36° 44' W	1° 12' S	0.014	0.033	0.393	0.025
95	36° 18' W	0° 54' S	0.015	0.033	0.393	0.025
96	36° 41' W	0° 28' S	0.016	0.033	0.393	0.025
97	36° 45' W	0° 08' N	0.017	0.033	0.393	0.025
98	37° 42' W	1° 45' N	0.024	0.020	0.416	0.024
99	Encke B crater	North rim	0.023	0.005	0.217	0.045
100	Encke B crater	NE rim	0.021	0.005	0.238	0.042
101	Encke B crater	East rim	0.020	0.005	0.250	0.040
102	Encke B crater	SE rim	0.020	0.005	0.250	0.040
103	Encke B crater	South rim	0.020	0.005	0.250	0.040
104	Encke B crater	SW rim	0.020	0.005	0.250	0.040
105	↑	West rim	0.020	0.005	0.250	0.040
106		NW rim	0.021	0.005	0.238	0.042
107	Encke crater	North rim	0.024	0.007	0.292	0.037
108	Encke crater	NE rim	0.023	0.007	0.292	0.037
109	Encke crater	East rim	0.022	0.007	0.292	0.037
110	Encke crater	SE rim	0.023	0.007	0.292	0.037
111	Encke crater	South rim	0.023	0.007	0.292	0.037
112	Encke crater	SW rim	0.024	0.007	0.292	0.037
113	Encke crater	West rim	0.025	0.007	0.292	0.037
114	Encke crater	NW rim	0.024	0.007	0.292	0.037
115	Kepler crater	North rim	0.035	0.004	0.114	0.088
116	Kepler crater	NE rim	0.033	0.004	0.121	0.083
117	Kepler crater	East rim	0.032	0.004	0.125	0.080
118	Kepler crater	SE rim	0.032	0.004	0.125	0.080
119	Kepler crater	South rim	0.032	0.004	0.125	0.080
120	Kepler crater	SW rim	0.034	0.004	0.118	0.085
121	Kepler crater	West rim	0.036	0.004	0.111	0.090
122	Kepler crater	NW rim	0.035	0.004	0.114	0.088
123	35° 37' W	10° 18' S	0.024	0.005	0.208	0.048
124	34° 20' W	10° 15' S	0.022	0.005	0.227	0.044
125	34° 15' W	9° 55' S	0.021	0.005	0.238	0.042
126	34° 15' W	9° 40' S	0.020	0.005	0.250	0.040
127	34° 27' W	4° 55' S	0.016	0.005	0.313	0.032
128	35° 00' W	4° 44' S	0.016	0.005	0.313	0.032
129	35° 31' W	4° 17' S	0.016	0.005	0.313	0.032
130	35° 53' W	4° 04' S	0.016	0.005	0.313	0.032
131	34° 45' W	4° 15' S	0.016	0.005	0.313	0.032
132	35° 11' W	4° 08' S	0.016	0.005	0.313	0.032
133	35° 33' W	3° 42' S	0.016	0.005	0.313	0.032
134	35° 59' W	3° 28' S	0.016	0.005	0.313	0.032
135	34° 19' W	4° 13' S	0.016	0.005	0.313	0.032
136	35° 22' W	3° 30' S	0.016	0.005	0.313	0.032
137	35° 23' W	2° 38' S	0.016	0.005	0.313	0.032
138	34° 19' W	3° 25' S	0.016	0.005	0.313	0.032
139	34° 41' W	2° 52' S	0.016	0.005	0.313	0.032
140	35° 09' W	2° 49' S	0.016	0.005	0.313	0.032
141	35° 39' W	2° 25' S	0.016	0.005	0.313	0.032
142	34° 50' W	2° 20' S	0.017	0.005	0.341	0.029
143	35° 03' W	1° 50' S	0.017	0.005	0.341	0.029
144	35° 08' W	1° 30' S	0.017	0.005	0.341	0.029
145	35° 15' W	1° 00' S	0.017	0.005	0.341	0.029
146	35° 24' W	0° 41' S	0.017	0.005	0.341	0.029
147	35° 34' W	0° 18' S	0.017	0.005	0.341	0.029
148	35° 50' W	0° 00'	0.017	0.005	0.341	0.029
149	33° 02' W	9° 40' S	0.022	0.010	0.454	0.022
150	33° 08' W	9° 17' S	0.022	0.010	0.454	0.022
151	35° 10' W	8° 42' S	0.021	0.009	0.429	0.021
152	33° 21' W	8° 05' S	0.020	0.009	0.450	0.022
153	32° 52' W	7° 28' S	0.019	0.009	0.473	0.021
154	32° 22' W	6° 32' S	0.018	0.008	0.444	0.023
155	33° 43' W	7° 00' S	0.017	0.008	0.470	0.021
156	33° 43' W	6° 40' S	0.016	0.008	0.500	0.020

TABLE 4 (continued)

Equivalent albedo for elevations determined from the effective temperatures given by SURVEYOR

Numerical order of elevations	Coordinates			The slope η/N	Temperature for the elevation	$\frac{N}{\eta}\delta\hat{T}_0$	Range of equivalent albedo
	Longitude	Latitude					
157	33° 38' W	6° 12' S		0.015	0.007	0.466	0.021
158	33° 06' W	6° 00' S		0.015	0.007	0.466	0.021
159	32° 48' W	5° 31' S		0.014	0.007	0.500	0.020
160	33° 07' W	5° 11' S		0.014	0.006	0.428	0.023
161	33° 36' W	4° 50' S		0.013	0.006	0.461	0.022
162	33° 28' W	4° 15' S		0.013	0.006	0.461	0.022
163	33° 12' W	4° 00' S		0.013	0.006	0.462	0.021
164	KUWAE CRATER	North	rim	0.019	0.005	0.263	0.380
165	KUWAE CRATER	NE	rim	0.018	0.005	0.277	0.035
166	KUWAE CRATER	East	rim	0.018	0.005	0.277	0.035
167	KUWAE CRATER	SE	rim	0.018	0.005	0.277	0.035
168	KUWAE CRATER	South	rim	0.018	0.005	0.277	0.035
169	KUWAE CRATER	SW	rim	0.019	0.005	0.263	0.380
170	KUWAE CRATER	West	rim	0.019	0.005	0.263	0.380
171	KUWAE CRATER	NW	rim	0.019	0.005	0.263	0.380
172	31° 58' W	9° 46' S		0.019	0.002	0.105	0.095
173	31° 42' W	9° 32' S		0.019	0.002	0.105	0.095
174	31° 49' W	9° 05' S		0.018	0.002	0.111	0.090
175	31° 15' W	8° 33' S		0.018	0.002	0.111	0.090
176	30° 37' W	8° 38' S		0.018	0.002	0.111	0.090
177	30° 17' W	9° 22' S		0.019	0.002	0.105	0.095
178	30° 25' W	9° 40' S		0.019	0.002	0.105	0.095
179	30° 11' W	5° 35' S		0.015	0.007	0.466	0.021
180	30° 42' W	5° 15' S		0.015	0.007	0.466	0.021
181	31° 10' W	4° 42' S		0.015	0.007	0.466	0.021
182	31° 12' W	4° 36' S		0.015	0.007	0.466	0.021
183	31° 33' W	4° 35' S		0.015	0.007	0.466	0.021
184	LANGSBERG Crater	North	rim	0.016	0.003	0.187	0.053
185	LANGSBERG Crater	NE	rim	0.016	0.003	0.187	0.053
186	LANGSBERG Crater	East	rim	0.016	0.003	0.187	0.053
187	LANGSBERG Crater	SE	rim	0.016	0.003	0.187	0.053
188	LANGSBERG Crater	South	rim	0.016	0.003	0.187	0.053
189	LANGSBERG Crater	SW	rim	0.016	0.003	0.187	0.053
190	LANGSBERG Crater	West	rim	0.016	0.003	0.187	0.053
191	LANGSBERG Crater	NW	rim	0.016	0.003	0.187	0.053
192	HORTENSIUS Crater	North	rim	0.019	0.003	0.157	0.063
193	HORTENSIUS Crater	NE	rim	0.019	0.003	0.157	0.063
194	HORTENSIUS Crater	East	rim	0.019	0.003	0.157	0.063
195	HORTENSIUS Crater	SE	rim	0.019	0.003	0.157	0.063
196	HORTENSIUS Crater	South	rim	0.019	0.003	0.157	0.063
197	HORTENSIUS Crater	SW	rim	0.019	0.003	0.157	0.063
198	HORTENSIUS Crater	West	rim	0.019	0.003	0.157	0.063
199	HORTENSIUS Crater	NW	rim	0.019	0.003	0.157	0.063
200	28° 22' W	10° 32' S		0.018	0.010	0.555	0.018
201	29° 00' W	10° 21' S		0.018	0.010	0.555	0.018
202	29° 11' W	10° 00' S		0.018	0.010	0.555	0.018
203	29° 22' W	9° 36' S		0.018	0.010	0.555	0.018
204	29° 18' W	9° 12' S		0.017	0.010	0.588	0.017
205	29° 00' W	8° 37' S		0.017	0.010	0.588	0.017
206	28° 23' W	8° 14' S		0.017	0.010	0.588	0.017
207	28° 20' W	7° 45' S		0.017	0.010	0.588	0.017
208	28° 20' W	7° 17' S		0.017	0.010	0.588	0.017
209	28° 26' W	7° 00' S		0.016	0.010	0.625	0.016
210	28° 50' W	6° 34' S		0.016	0.010	0.625	0.016
211	28° 27' W	6° 12' S		0.016	0.010	0.625	0.016
212	28° 13' W	5° 43' S		0.016	0.010	0.625	0.016
213	28° 45' W	5° 32' S		0.016	0.010	0.625	0.016
214	29° 00' W	5° 23' S		0.015	0.010	0.666	0.015
215	29° 21' W	5° 04' S		0.015	0.010	0.666	0.015
216	28° 40' W	4° 40' S		0.015	0.010	0.666	0.015
217	28° 40' W	4° 19' S		0.015	0.010	0.666	0.015
218	27° 58' W	10° 25' S		0.018	0.010	0.555	0.018
219	27° 54' W	9° 40' S		0.018	0.010	0.555	0.018
220	27° 37' W	8° 59' S		0.018	0.010	0.555	0.018
221	27° 28' W	8° 33' S		0.017	0.010	0.588	0.017
222	27° 17' W	7° 55' S		0.017	0.010	0.588	0.017
223	26° 54' W	7° 33' S		0.017	0.010	0.588	0.017
224	26° 39' W	7° 15' S		0.017	0.010	0.588	0.017
225	27° 28' W	6° 18' S		0.017	0.010	0.588	0.017
226	27° 19' W	5° 38' S		0.017	0.010	0.588	0.017
227	LANGSBERG Crater	North	rim	0.015	0.007	0.466	0.022
228	LANGSBERG Crater	NE	rim	0.014	0.007	0.500	0.020
229	LANGSBERG Crater	East	rim	0.014	0.007	0.500	0.020
230	LANGSBERG Crater	SE	rim	0.014	0.007	0.500	0.020
231	LANGSBERG Crater	South	rim	0.014	0.007	0.500	0.020
232	LANGSBERG Crater	SW	rim	0.014	0.007	0.500	0.020
233	LANGSBERG Crater	West	rim	0.015	0.007	0.466	0.022
234	LANGSBERG Crater	NW	rim	0.015	0.007	0.466	0.022

TABLE 4 (continued)

Equivalent albedo for elevations determined from the effective temperatures given by SURVEYOR

Numerical order of elevations	Coordinates		the slope η/N	temperature fluctuation of the elevation	$\frac{N}{\eta}\delta T_0$	Range of equivalent albedo
	Longitude	Latitude				
235	24° 35' W	10° 30' S	0.017	0.002	0.117	0.085
236	24° 30' W	10° 00' S	0.017	0.002	0.117	0.085
237	24° 28' W	9° 45' S	0.017	0.002	0.117	0.085
238	24° 24' W	9° 42' S	0.017	0.002	0.117	0.085
239	24° 18' W	9° 12' S	0.016	0.002	0.125	0.080
240	24° 14' W	9° 00' S	0.016	0.002	0.125	0.080
241	24° 22' W	8° 50' S	0.016	0.002	0.125	0.080
242	24° 20' W	8° 28' S	0.016	0.002	0.125	0.080
243	24° 19' W	8° 12' S	0.016	0.002	0.125	0.080
244	24° 18' W	8° 00' S	0.016	0.002	0.125	0.080
245	24° 17' W	7° 41' S	0.015	0.002	0.133	0.075
246	24° 13' W	7° 28' S	0.015	0.002	0.133	0.075
247	24° 12' W	7° 12' S	0.015	0.002	0.133	0.075
248	24° 10' W	7° 00' S	0.015	0.002	0.133	0.075
249	24° 07' W	6° 45' S	0.015	0.002	0.133	0.075
250	24° 05' W	6° 33' S	0.015	0.002	0.133	0.075
251	Crater HORTENSIUS	North rim	0.017	0.005	0.294	0.034
252	"	NE rim	0.017	0.005	0.294	0.034
253	"	East rim	0.017	0.005	0.294	0.034
254	"	SE rim	0.017	0.005	0.294	0.034
255	"	South rim	0.017	0.005	0.294	0.034
256	"	SW rim	0.017	0.005	0.294	0.034
257	"	West rim	0.017	0.005	0.294	0.034
258	"	NW rim	0.017	0.005	0.294	0.034
259	23° 53' W	7° 00' S	0.015	0.002	0.133	0.075
260	23° 42' W	6° 48' S	0.015	0.002	0.133	0.075
261	23° 30' W	6° 29' S	0.015	0.002	0.133	0.075
262	23° 19' W	6° 17' S	0.015	0.002	0.133	0.075
263	23° 17' W	6° 00' S	0.014	0.002	0.143	0.070
264	23° 05' W	5° 43' S	0.014	0.002	0.143	0.070
265	22° 33' W	5° 22' S	0.014	0.002	0.143	0.070
266	Crater REINHOLD	North rim	0.016	0.007	0.437	0.023
267	"	NE rim	0.016	0.007	0.437	0.023
268	"	East rim	0.016	0.007	0.437	0.023
269	"	SE rim	0.016	0.007	0.437	0.023
270	"	South rim	0.016	0.007	0.437	0.023
271	"	SW rim	0.016	0.007	0.437	0.023
272	"	West rim	0.016	0.007	0.437	0.023
273	"	NW rim	0.016	0.007	0.437	0.023
274	21° 16' W	10° 55' S	0.018	0.002	0.111	0.090
275	21° 05' W	10° 43' S	0.017	0.002	0.117	0.085
276	20° 54' W	10° 34' S	0.016	0.002	0.125	0.080
277	20° 40' W	10° 00' S	0.016	0.002	0.125	0.080
278	20° 29' W	9° 30' S	0.015	0.002	0.133	0.075
279	20° 00' W	7° 57' S	0.015	0.002	0.133	0.075
280	20° 00' W	7° 48' S	0.014	0.002	0.143	0.070
281	20° 00' W	7° 32' S	0.014	0.002	0.143	0.070
282	20° 00' W	6° 59' S	0.013	0.002	0.154	0.065
283	20° 00' W	6° 40' S	0.013	0.002	0.154	0.065
284	20° 00' W	6° 25' S	0.012	0.002	0.166	0.060
285	21° 05' W	3° 35' S	0.012	0.002	0.166	0.060
286	20° 58' W	3° 18' S	0.011	0.002	0.181	0.055
287	20° 33' W	2° 40' S	0.011	0.002	0.181	0.055
288	20° 30' W	2° 35' S	0.011	0.002	0.181	0.055
289	Crater FAUTH	North rim	0.016	0.005	0.313	0.032
290	"	NE rim	0.016	0.005	0.313	0.032
291	"	East rim	0.016	0.005	0.313	0.032
292	"	SE rim	0.016	0.005	0.313	0.032
293	"	South rim	0.016	0.005	0.313	0.032
294	"	SW rim	0.016	0.005	0.313	0.032
295	"	West rim	0.016	0.005	0.313	0.032
296	"	NW rim	0.016	0.005	0.313	0.032
297	Crater COPERNICUS	North rim	0.016	0.007	0.437	0.023
298	"	NE rim	0.016	0.007	0.437	0.023
299	"	East rim	0.016	0.007	0.437	0.023
300	"	SE rim	0.016	0.007	0.437	0.023
301	"	South rim	0.016	0.007	0.437	0.023
302	"	SW rim	0.016	0.007	0.437	0.023
303	"	West rim	0.016	0.007	0.437	0.023
304	"	NW rim	0.016	0.007	0.437	0.023
305	Crater KEPLER	North rim	0.016	0.007	0.437	0.023
306	"	NE rim	0.016	0.007	0.437	0.023
307	"	East rim	0.016	0.007	0.437	0.023
308	"	SE rim	0.016	0.007	0.437	0.023
309	"	South rim	0.016	0.007	0.437	0.023
310	"	SW rim	0.016	0.007	0.437	0.023
311	"	West rim	0.016	0.007	0.437	0.023
312	"	NW rim	0.016	0.007	0.437	0.023

TABLE 5

Equivalent albedo for relatively flat surface determined from the effective temperatures given by SURVEYOR

Numerical order of points	Coordinates		The slope η/N	Temperature at the point of the surface	$\frac{N}{\eta}\delta\hat{T}_0$	Range of equivalent albedo
	Longitude	Latitude				
1	43°14'W	1°00'S	0.100	0.001	0.010	1.000
2	43°14'W	0°52'S	0.100	0.001	0.010	1.000
3	43°14'W	0°33'S	0.100	0.001	0.010	1.000
4	43°14'W	0°16'S	0.100	0.001	0.010	1.000
5	43°14'W	0°10'N	0.100	0.001	0.010	1.000
6	42°58'W	0°52'S	0.060	0.001	0.017	0.588
7	42°58'W	0°33'S	0.095	0.001	0.010	1.000
8	42°58'W	0°16'S	0.077	0.001	0.013	0.769
9	42°58'W	0°10'N	0.088	0.001	0.011	0.909
10	42°42'W	0°33'S	0.057	0.001	0.018	0.555
11	42°42'W	0°16'S	0.073	0.001	0.014	0.714
12	42°42'W	0°00'	0.062	0.001	0.016	0.625
13	43°14'W	3°05'N	0.100	0.001	0.010	1.000
14	43°14'W	3°05'N	0.100	0.001	0.010	1.000
15	43°14'W	3°34'N	0.100	0.001	0.010	1.000
16	43°14'W	4°05'N	0.100	0.001	0.010	1.000
17	42°42'W	3°05'N	0.088	0.001	0.011	0.909
18	42°42'W	3°15'N	0.088	0.001	0.011	0.909
19	42°42'W	3°34'N	0.088	0.001	0.011	0.909
20	42°42'W	4°05'N	0.088	0.001	0.011	0.909
21	41°30'W	0°07'N	0.033	0.001	0.030	0.333
22	41°43'W	0°26'N	0.036	0.001	0.028	0.357
23	41°43'W	0°38'N	0.038	0.001	0.026	0.384
24	41°43'W	1°03'N	0.039	0.001	0.026	0.384
25	41°43'W	1°35'N	0.041	0.001	0.024	0.417
26	41°43'W	2°00'N	0.043	0.001	0.023	0.435
27	41°13'W	0°30'N	0.030	0.001	0.033	0.303
28	41°13'W	0°42'N	0.032	0.001	0.031	0.322
29	41°13'W	1°13'N	0.035	0.001	0.029	0.356
30	41°13'W	1°35'N	0.038	0.001	0.026	0.384
31	41°13'W	1°56'N	0.038	0.001	0.026	0.384
32	39°24'W	1°25'S	0.041	0.001	0.024	0.417
33	39°24'W	1°03'S	0.040	0.001	0.025	0.400
34	39°24'W	0°42'S	0.038	0.001	0.026	0.384
35	39°00'W	1°25'S	0.036	0.001	0.028	0.357
36	39°00'W	1°03'S	0.036	0.001	0.028	0.357
37	39°00'W	0°42'S	0.039	0.001	0.026	0.384
38	38°30'W	1°28'S	0.041	0.001	0.024	0.417
39	38°30'W	1°07'S	0.044	0.001	0.023	0.435
40	38°30'W	0°40'S	0.048	0.001	0.021	0.476
41	37°42'W	2°07'S	0.050	0.001	0.020	0.500
42	37°42'W	1°43'S	0.014	0.001	0.071	0.141
43	37°42'W	1°30'S	0.015	0.001	0.066	0.156
44	37°42'W	1°00'S	0.016	0.001	0.063	0.158
45	37°42'W	1°34'S	0.017	0.001	0.058	0.172
46	37°42'W	1°12'S	0.018	0.001	0.055	0.181
47	37°15'W	2°07'S	0.014	0.001	0.071	0.141
48	37°15'W	1°43'S	0.016	0.001	0.063	0.158
49	37°15'W	1°30'S	0.016	0.001	0.063	0.158
50	37°15'W	1°00'S	0.017	0.001	0.058	0.172
51	37°15'W	1°34'S	0.018	0.001	0.055	0.181
52	37°15'W	1°12'S	0.018	0.001	0.055	0.181
53	36°22'W	4°07'S	0.016	0.001	0.063	0.158
54	36°22'W	3°48'S	0.015	0.001	0.066	0.156
55	36°22'W	3°19'S	0.014	0.001	0.071	0.141
56	36°22'W	3°27'S	0.014	0.001	0.071	0.141
57	36°41'W	4°07'S	0.016	0.001	0.063	0.158
58	36°41'W	3°48'S	0.015	0.001	0.066	0.156
59	36°41'W	3°19'S	0.015	0.001	0.066	0.156
60	36°41'W	3°27'S	0.014	0.001	0.071	0.141
61	34°41'W	3°08'N	0.019	0.001	0.052	0.192
62	34°41'W	3°25'N	0.019	0.001	0.052	0.192
63	34°41'W	3°50'N	0.019	0.001	0.052	0.192
64	34°17'W	3°08'N	0.019	0.001	0.052	0.192
65	34°17'W	3°25'N	0.019	0.001	0.052	0.192
66	34°17'W	3°50'N	0.019	0.001	0.052	0.192
67	35°22'W	11°30'S	0.029	0.001	0.034	0.294
68	35°22'W	11°30'S	0.028	0.001	0.035	0.286
69	35°22'W	10°50'S	0.027	0.001	0.037	0.270
70	35°05'W	11°30'S	0.026	0.001	0.038	0.263
71	35°05'W	11°15'S	0.025	0.001	0.040	0.250
72	35°05'W	10°50'S	0.023	0.001	0.043	0.233
73	34°40'W	11°30'S	0.023	0.001	0.043	0.233
74	34°40'W	11°15'S	0.023	0.001	0.043	0.233
75	34°40'W	10°50'S	0.023	0.001	0.043	0.233
76	35°15'W	7°35'S	0.021	0.001	0.046	0.217
77	35°15'W	7°20'S	0.020	0.001	0.050	0.200
78	35°15'W	6°50'S	0.019	0.001	0.052	0.192

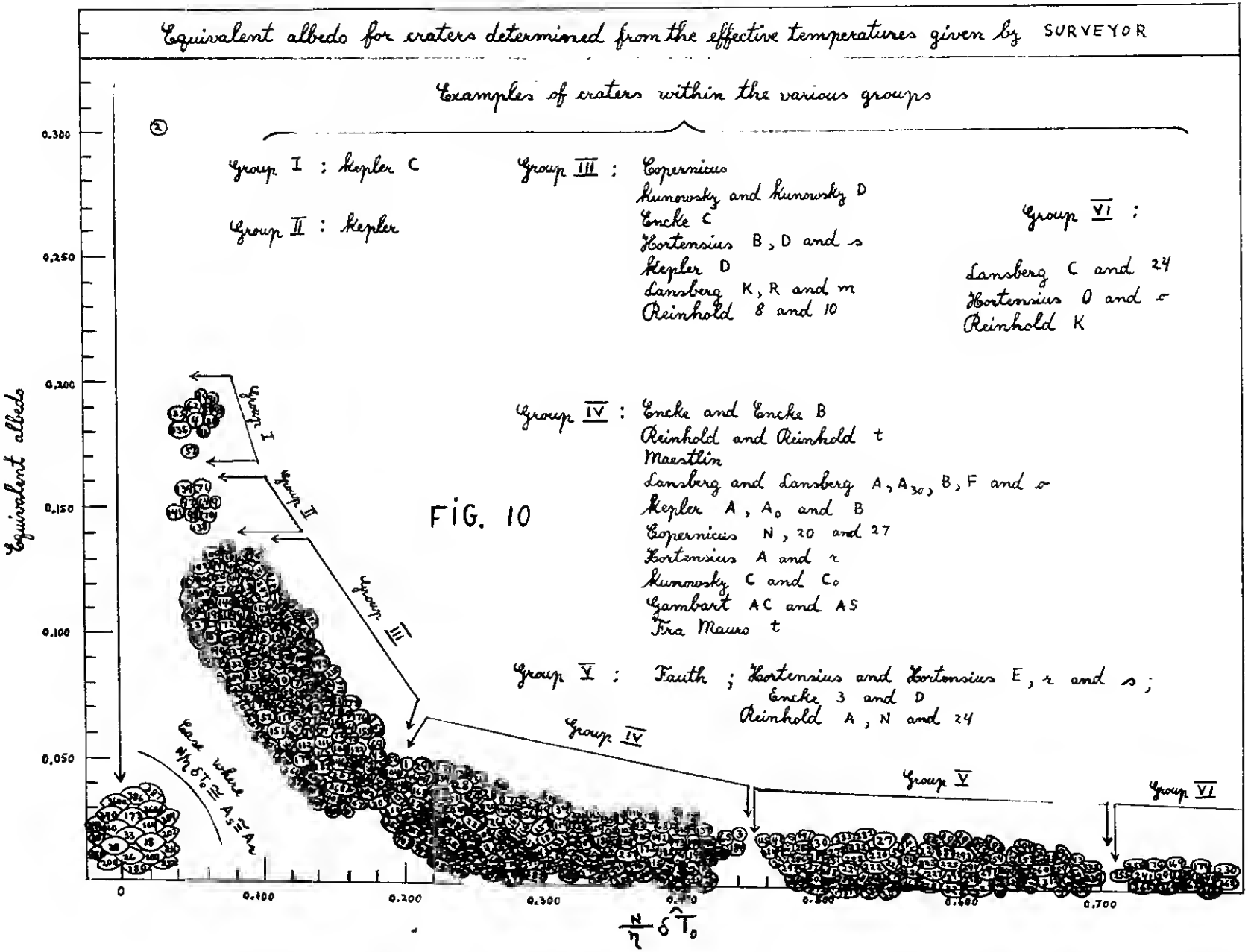
Equivalent albedo for craters determined from the effective temperatures given by SURVEYOR
Examples of craters within the various groups
Group I : Kepler C
Group II : Kepler
Group III : Copernicus
Kunowsky and Kunowsky D
Encke C
Hortensius B, D and s
Kepler D
Lansberg K, R and m
Reinhold 8 and 10
Group VI :
Lansberg C and 24
Hortensius O and o
Reinhold K
Group IV : Encke and Encke B
Reinhold and Reinhold t
Maestlin
Lansberg and Lansberg A, A30, B, F and o
Kepler A, A0 and B
Copernicus N, 20 and 27
Hortensius A and r
Kunowsky C and C0
Gambart AC and AS
Fra Mauro t
Group V : Fauth ; Hortensius and Hortensius E, r and s ;
Encke 3 and D
Reinhold A, N and 24
Equivalent albedo
0.300
0.250
0.200
0.150
0.100
0.050
Group I
Group II
Group III
Group IV
Group V
Group VI
Here where
0
0.100
0.200
0.300
0.400
0.500
0.600
0.700

FIG. 10

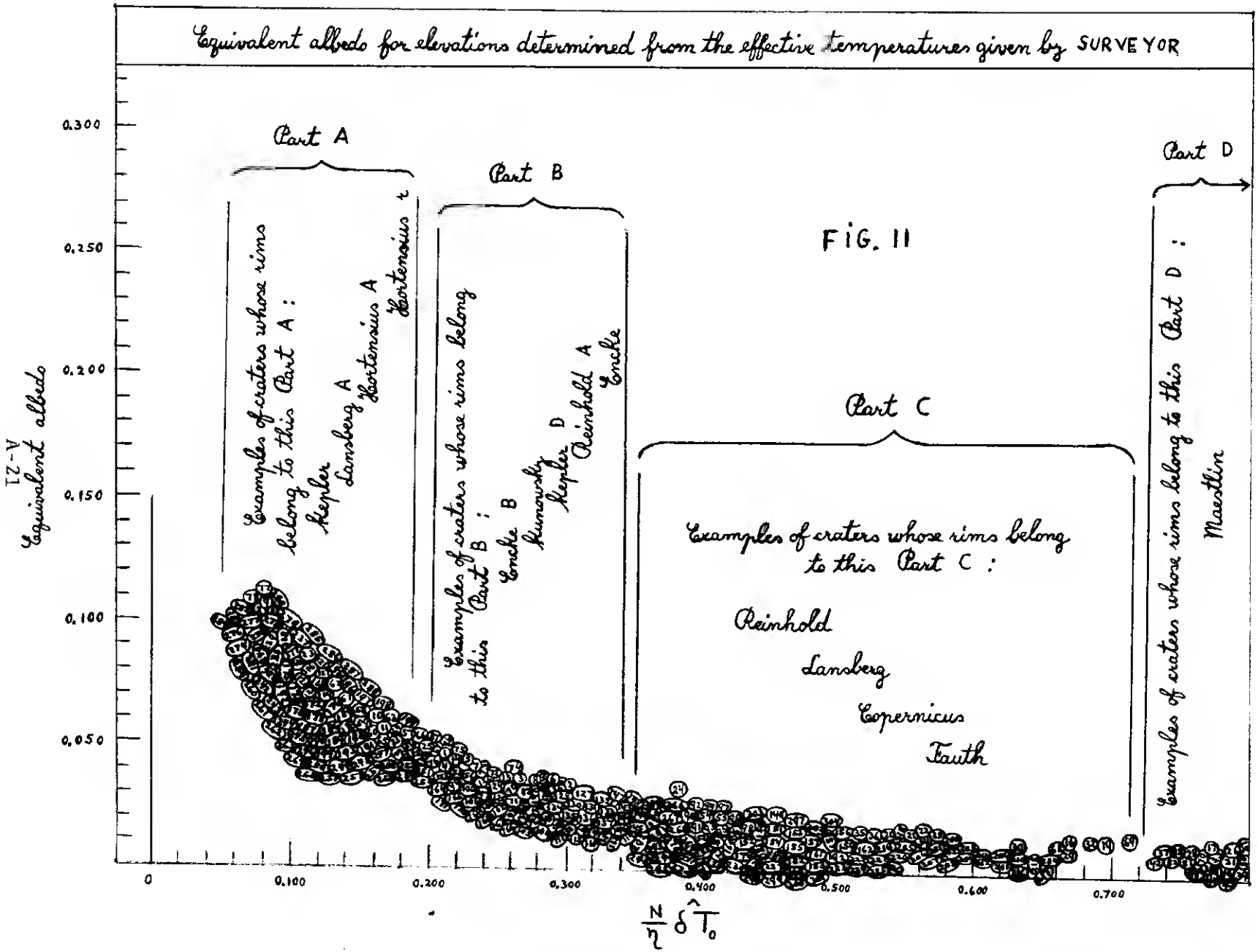
Equivalent albedos for elevations determined from the effective temperatures given by SURVEYOR
Part A
Part B
Part C
Part D
Examples of craters whose rims belong to this Part A :
Kepler
Lansberg A
Hortensius A
Hortensius t
Examples of craters whose rims belong to this Part B :
Encke B
Kunowsky
Kepler D
Reinhold A
Encke
Examples of craters whose rims belong to this Part C :
Reinhold
Lansberg
Copernicus
Tauth
Examples of craters whose rims belong to this Part D :
Maestlin
Equivalent albedo
A-21
0.300
0.250
0.200
0.150
0.100
0.050
0
0.100
0.200
0.300
0.400
0.500
0.600
0.700
$\frac{N}{\eta}\delta\hat{T}_0$

FIG. 11

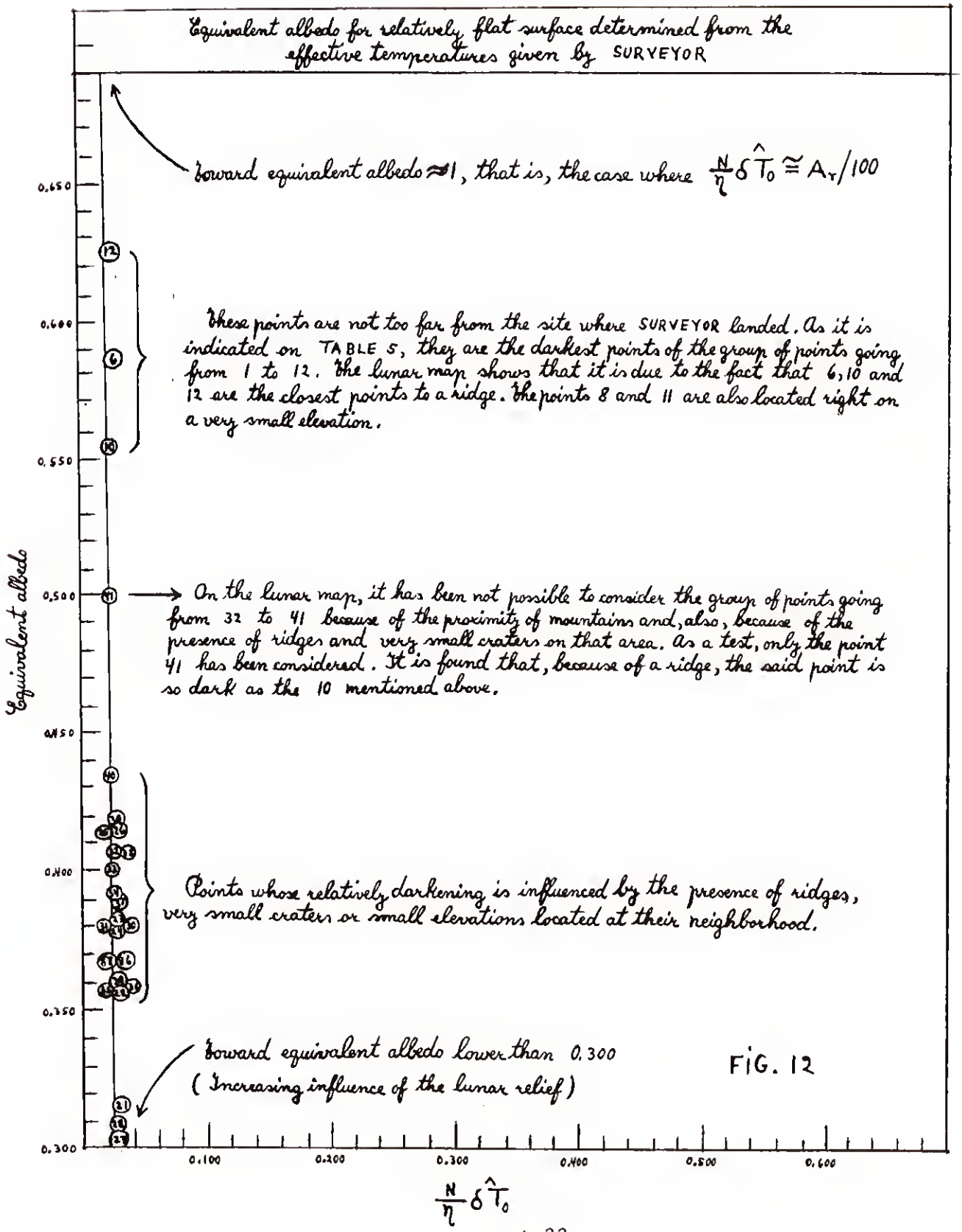
Equivalent albedo for relatively flat surface determined from the effective temperatures given by SURVEYOR
Toward equivalent albedo ≈1, that is, the case where $\frac{N}{\eta}\delta\hat{T}_0 \cong A_r/100$
These points are not too far from the site where SURVEYOR landed. As it is indicated on TABLE 5, they are the darkest points of the group of points going from 1 to 12. The lunar map shows that it is due to the fact that 6, 10 and 12 are the closest points to a ridge. The points 8 and 11 are also located right on a very small elevation.
On the lunar map, it has been not possible to consider the group of points going from 32 to 41 because of the proximity of mountains and, also, because of the presence of ridges and very small craters on that area. As a test, only the point 41 has been considered. It is found that, because of a ridge, the said point is so dark as the 10 mentioned above.
Points whose relatively darkening is influenced by the presence of ridges, very small craters or small elevations located at their neighborhood.
Toward equivalent albedo lower than 0.300
(Increasing influence of the lunar relief)
Equivalent albedo
0.650
0.600
0.550
0.500
0.450
0.400
0.350
0.300
0.100
0.200
0.300
0.400
0.500
0.600
$\frac{N}{\eta}\delta\hat{T}_0$

FIG. 12

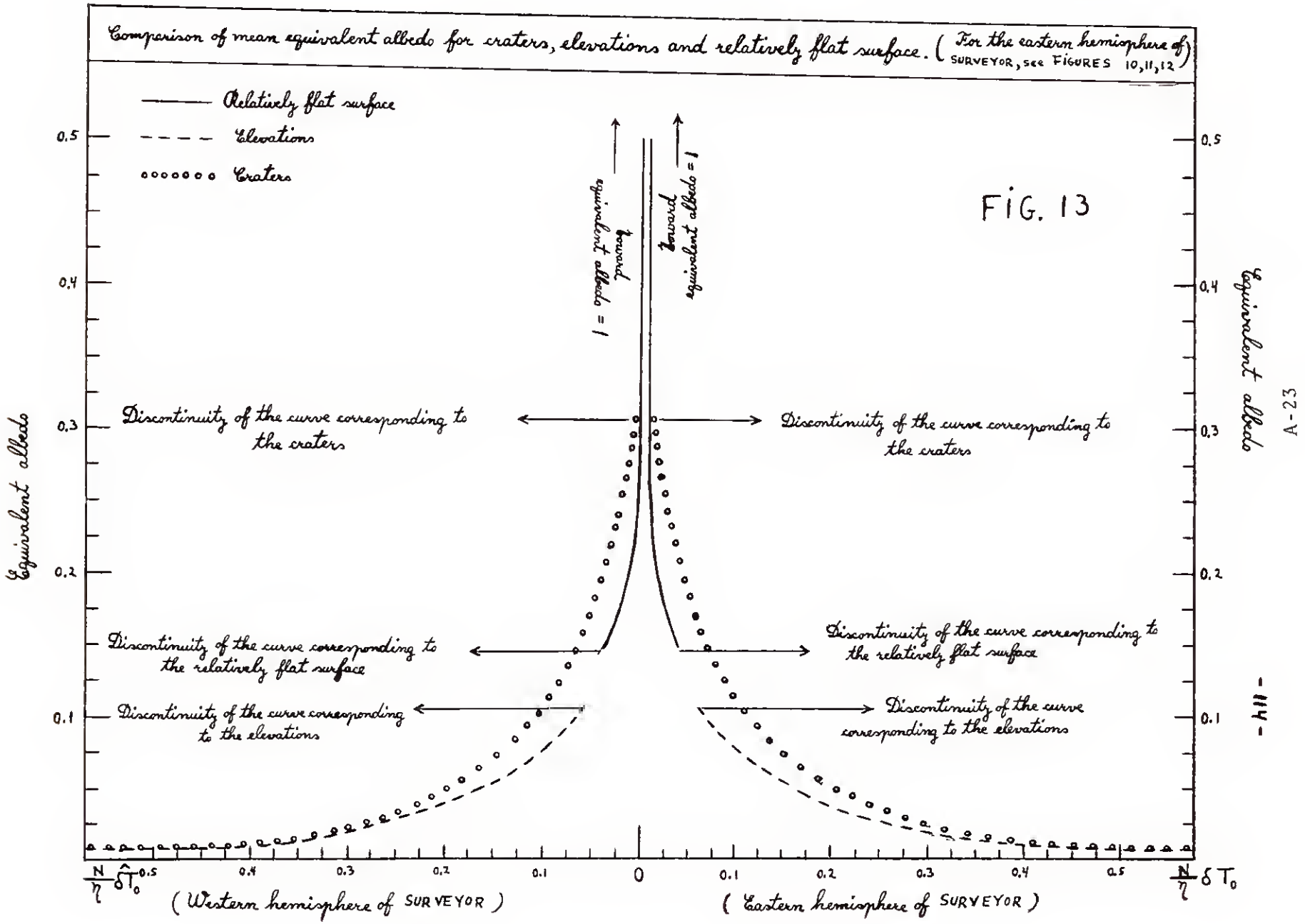
Comparison of mean equivalent albedo for craters, elevations and relatively flat surface. (For the eastern hemisphere of SURVEYOR, see FIGURES 10,11,12)
Relatively flat surface
Elevations
Craters
FIG. 13
Equivalent albedo
0.5
0.4
0.3
0.2
0.1
Forward equivalent albedo = 1
Forward equivalent albedo = 1
Discontinuity of the curve corresponding to the craters
Discontinuity of the curve corresponding to the craters
Discontinuity of the curve corresponding to the relatively flat surface
Discontinuity of the curve corresponding to the relatively flat surface
Discontinuity of the curve corresponding to the elevations
Discontinuity of the curve corresponding to the elevations
0.5
0.4
0.3
0.2
0.1
0
0.1
0.2
0.3
0.4
0.5
(Western hemisphere of SURVEYOR)
(Eastern hemisphere of SURVEYOR)

Examples of points considered for the eastern hemisphere of SURVEYOR (See FIGURES 10,11 and 12)

1, 2, 3, 4, etc. indicate craters ; $\frac{1}{}$, $\frac{2}{}$, $\frac{3}{}$, $\frac{4}{}$, indicate elevations ; ①, ②, ③, ④, etc. indicate relatively flat surface

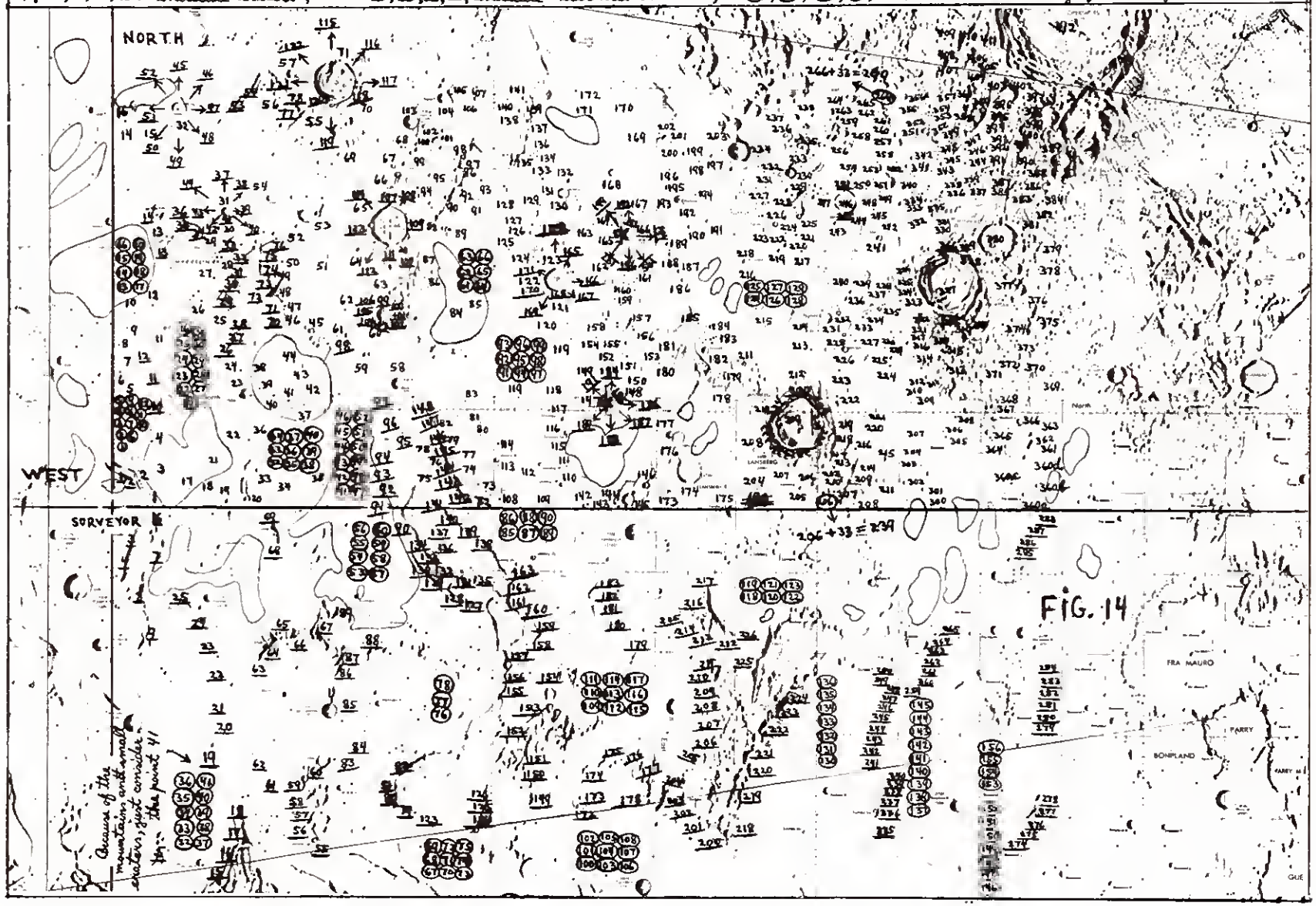

FIG. 14

Examples of craters whose equivalent albedo are equal to As and their possible influence on the anomalies of the effective temperatures contours.

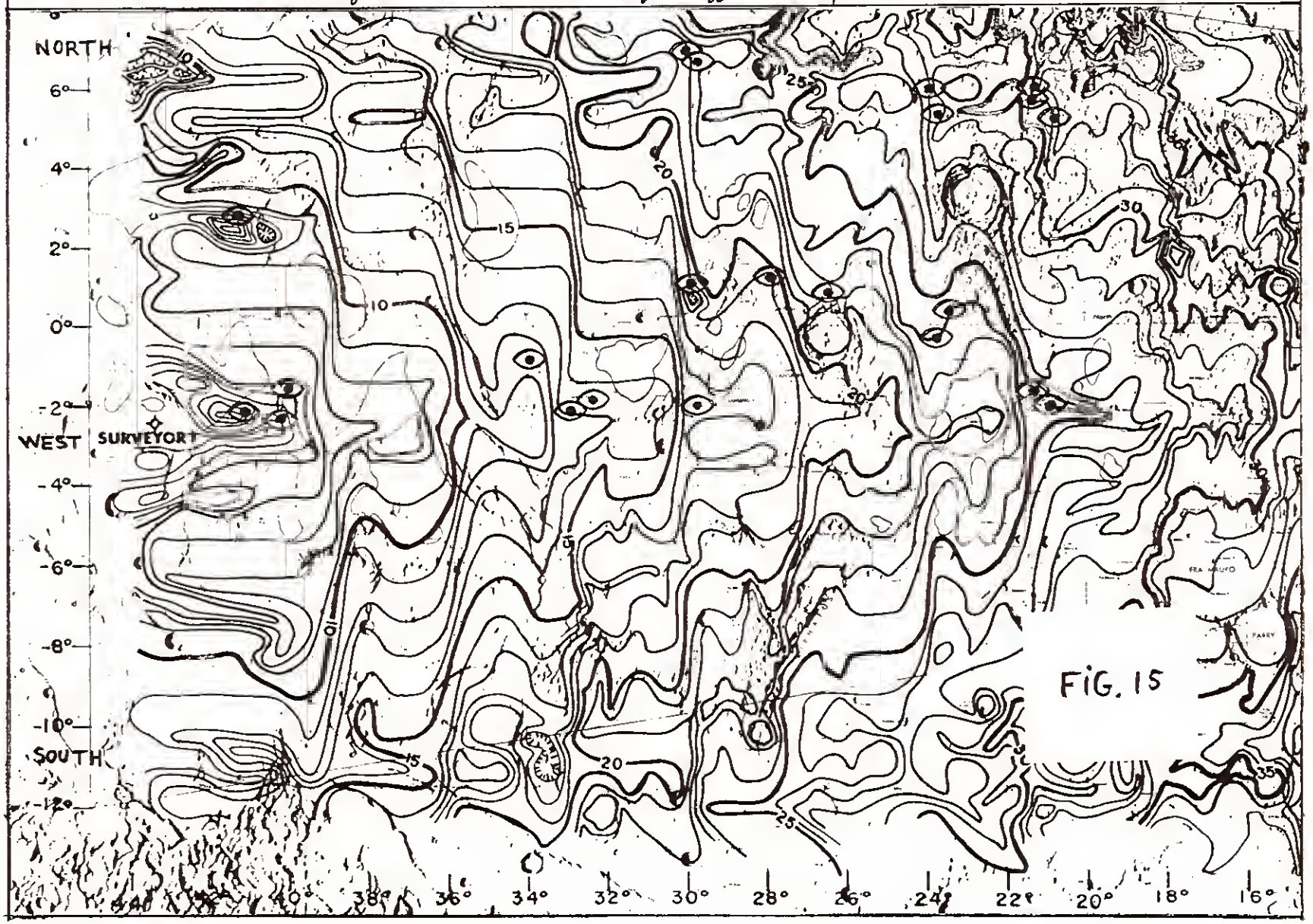

FIG. 15

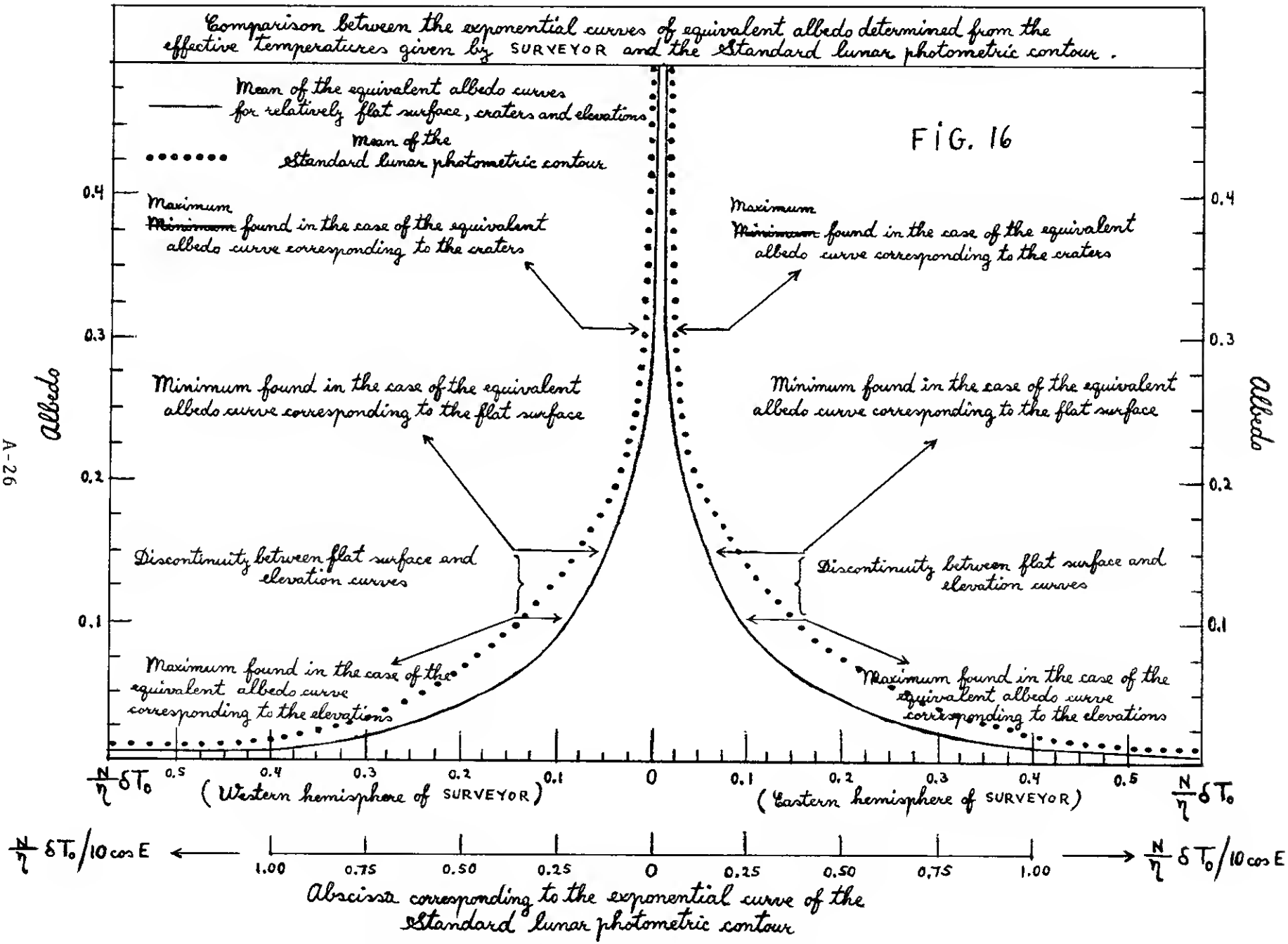
Comparison between the exponential curves of equivalent albedo determined from the effective temperatures given by SURVEYOR and the Standard lunar photometric contour.
Mean of the equivalent albedo curves for relatively flat surface, craters and elevations
Mean of the Standard lunar photometric contour
FIG. 16
Maximum found in the case of the equivalent albedo curve corresponding to the craters
Minimum found in the case of the equivalent albedo curve corresponding to the flat surface
Discontinuity between flat surface and elevation curves
Maximum found in the case of the equivalent albedo curve corresponding to the elevations
Albedo
0.4
0.3
0.2
0.1
0.5
0.4
0.3
0.2
0.1
0
(Western hemisphere of SURVEYOR)
(Eastern hemisphere of SURVEYOR)
$\frac{N}{\eta}\delta T_0$
$\frac{N}{\eta}\delta T_0/10\cos E$
1.00
0.75
0.50
0.25
Abscissa corresponding to the exponential curve of the Standard lunar photometric contour

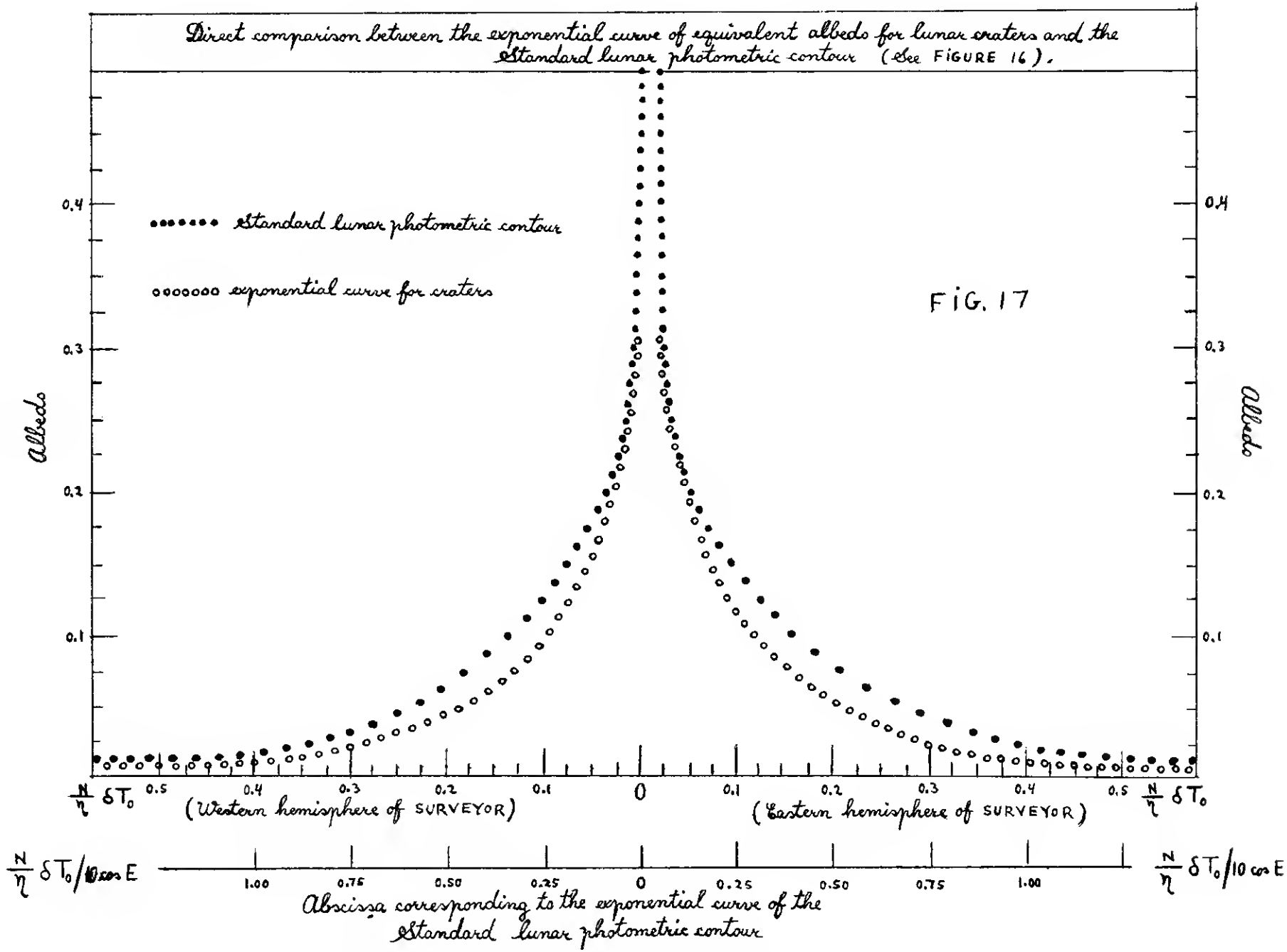
Direct comparison between the exponential curve of equivalent albedo for lunar craters and the standard lunar photometric contour (See FIGURE 16).
Standard lunar photometric contour
exponential curve for craters
FIG. 17
albedo
0.4
0.3
0.2
0.1
$\frac{N}{\eta}\delta T_0$
0.5 0.4 0.3 0.2 0.1 0 0.1 0.2 0.3 0.4 0.5
(Western hemisphere of SURVEYOR)
(Eastern hemisphere of SURVEYOR)
$\frac{N}{\eta}\delta T_0/10\cos E$
1.00 0.75 0.50 0.25 0 0.25 0.50 0.75 1.00
Abscissa corresponding to the exponential curve of the standard lunar photometric contour

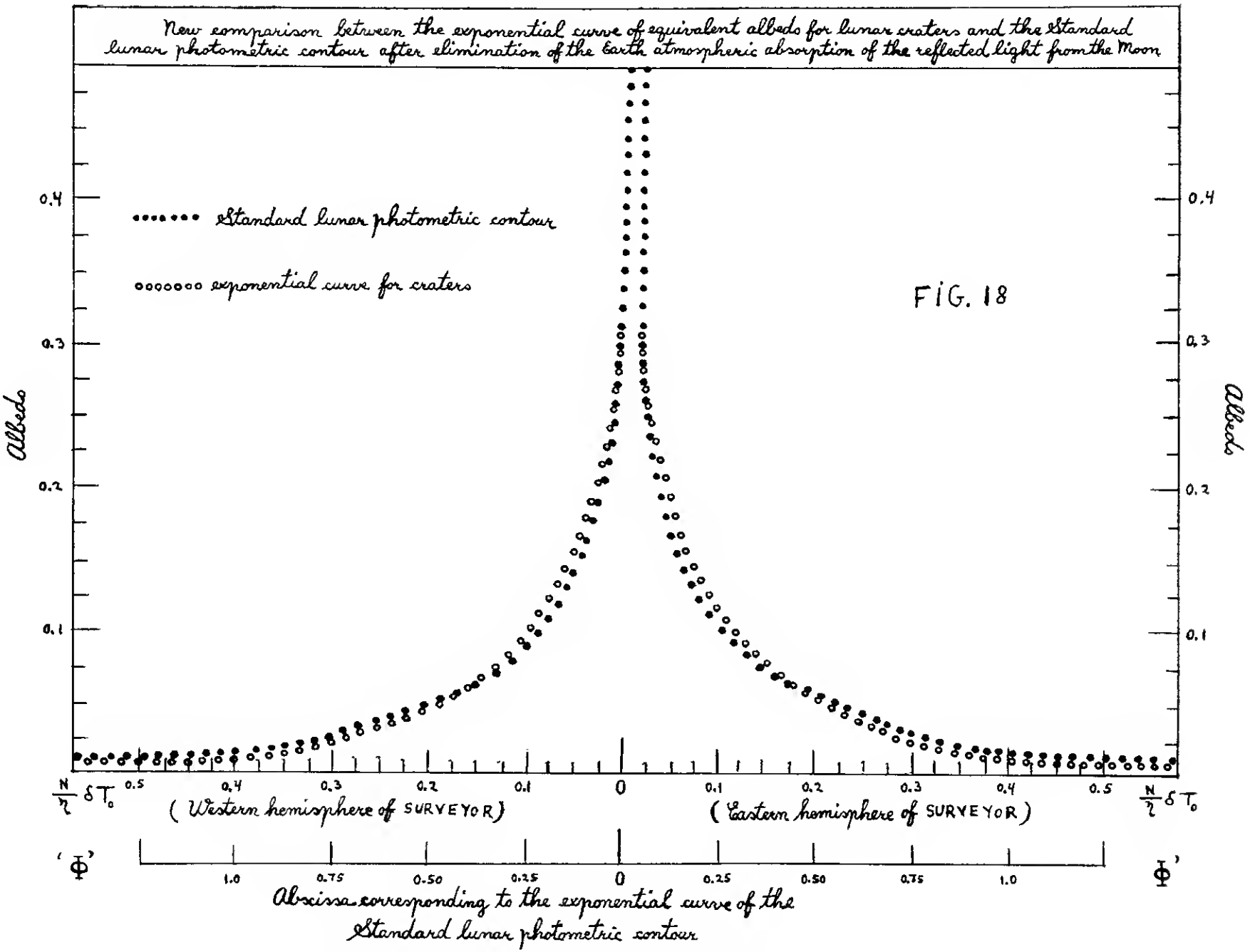
New comparison between the exponential curve of equivalent albedo for lunar craters and the Standard lunar photometric contour after elimination of the Earth atmospheric absorption of the reflected light from the Moon
Standard lunar photometric contour
exponential curve for craters
Albedo
0.4
0.3
0.2
0.1
$\frac{N}{r}\delta T_0$
0.5 0.4 0.3 0.2 0.1 0
(Western hemisphere of SURVEYOR)
(Eastern hemisphere of SURVEYOR)
Φ'
1.0 0.75 0.50 0.25 0
Abscissa corresponding to the exponential curve of the Standard lunar photometric contour

FIG. 18

Comparison of the equivalent albedo curves determined from the effective temperatures given by SURVEYOR for the different groups of craters of the FIGURE 10 .

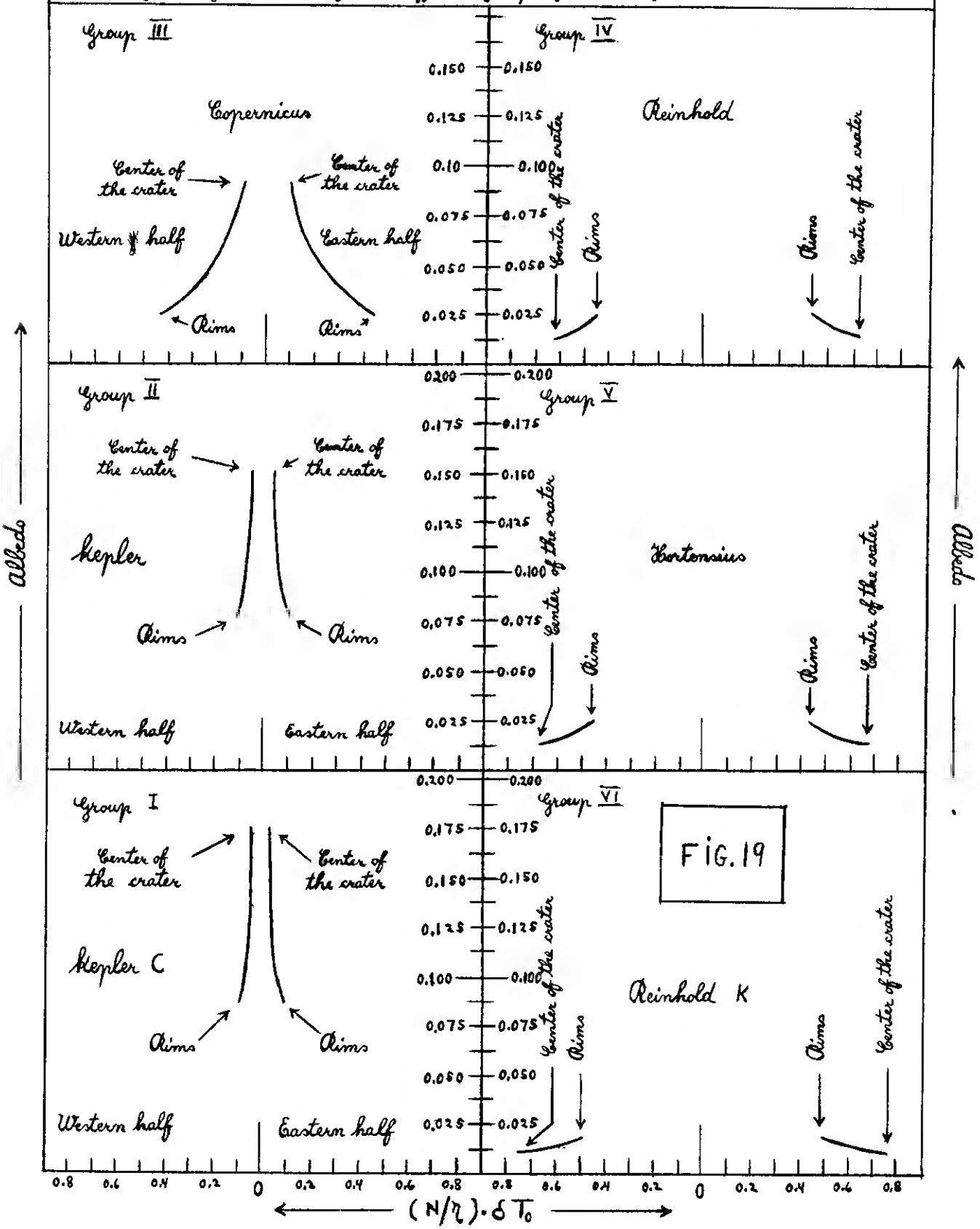

FIG. 19

Some examples about the difference between the craters of the groups I, II, III and those of the groups IV, V, VI.

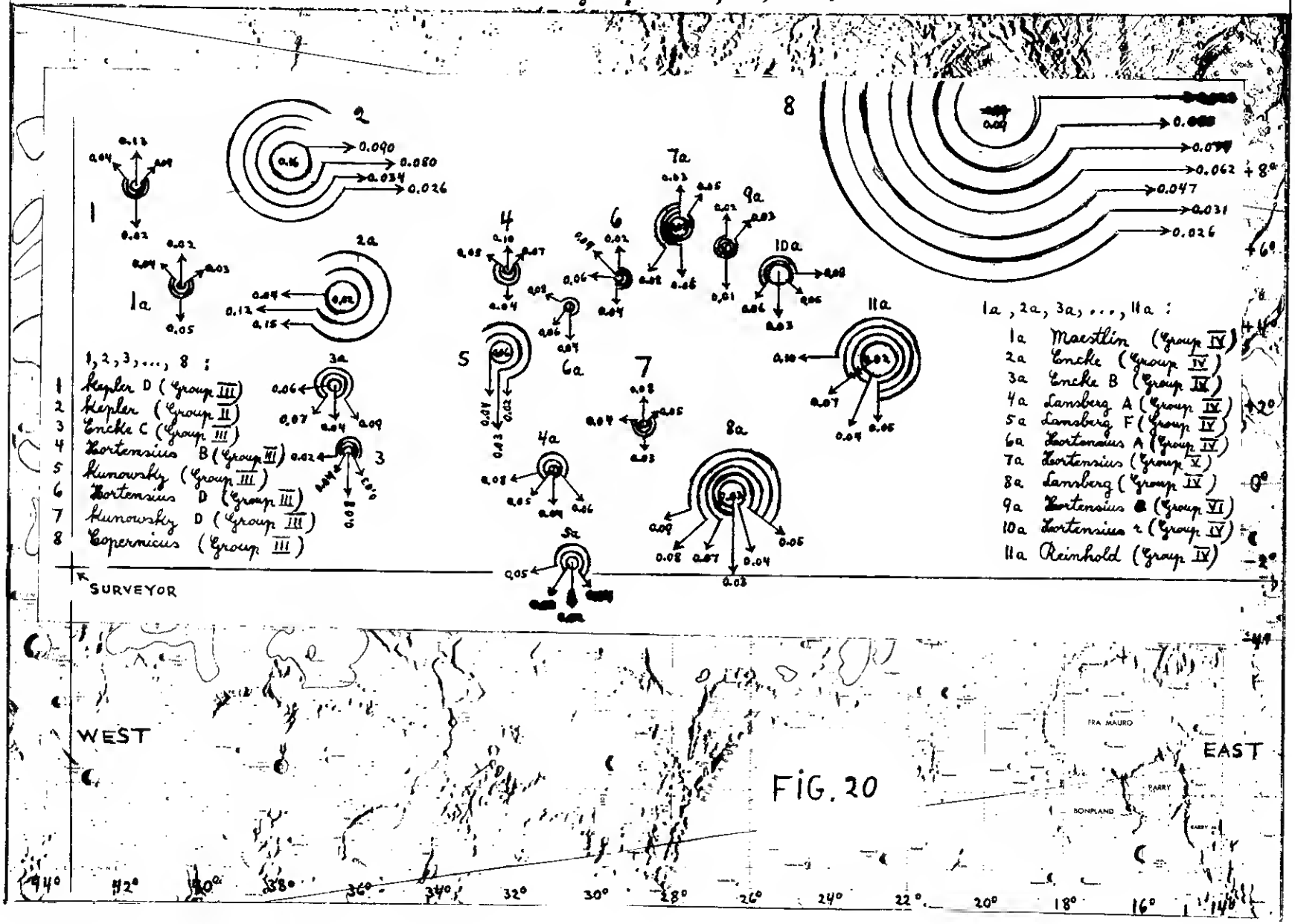

FIG. 20

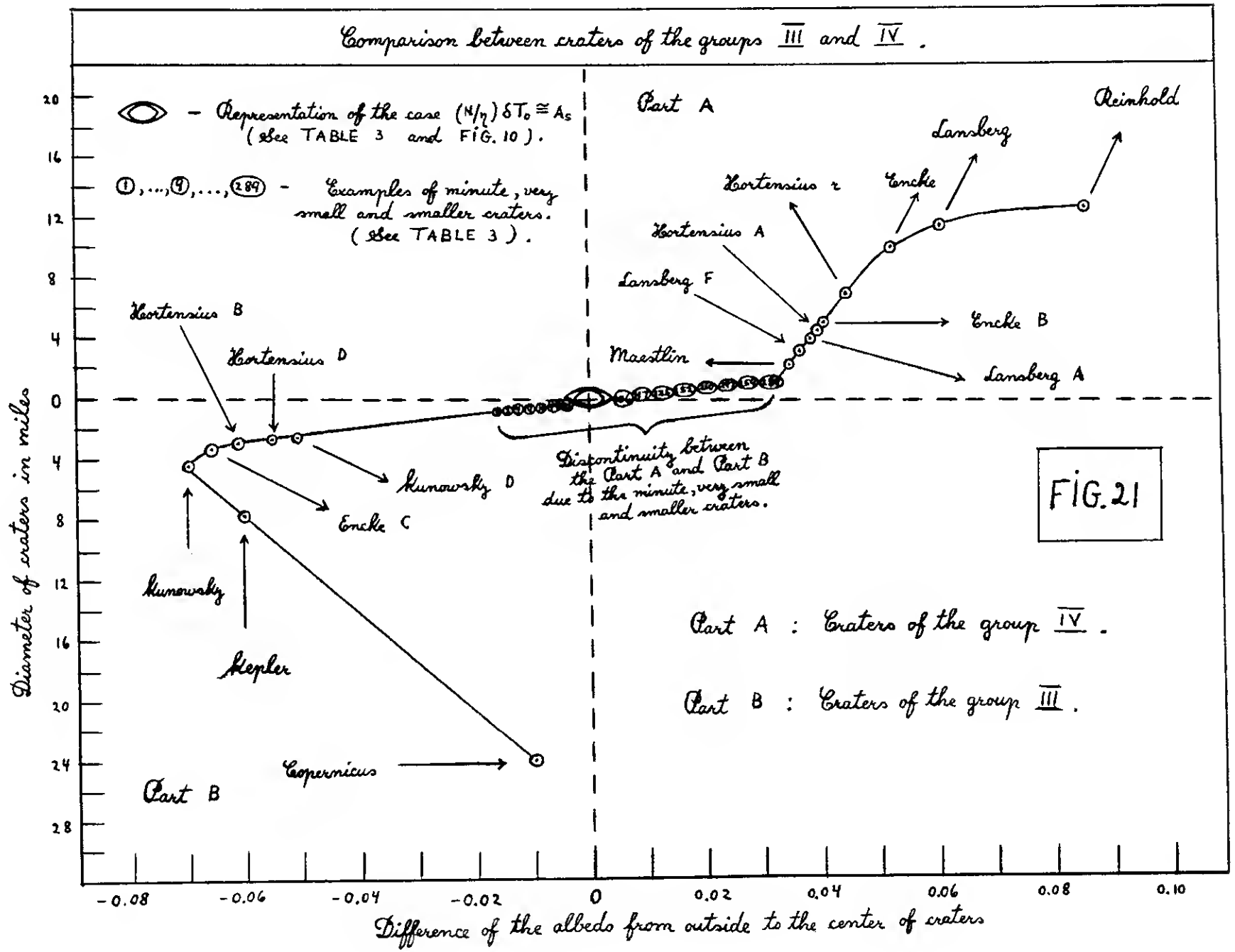
Comparison between craters of the groups III and IV .
Part A
Part B
– Representation of the case (N/η) δT₀ ≅ A_S (See TABLE 3 and FIG. 10).
①,...,⑨,...,289 – Examples of minute, very small and smaller craters. (See TABLE 3).
Reinhold
Lansberg
Hortensius r
Encke
Hortensius A
Lansberg F
Encke B
Maestlin
Lansberg A
Hortensius B
Hortensius D
Kunowsky D
Encke C
Kunowsky
Kepler
Copernicus
Discontinuity between the Part A and Part B due to the minute, very small and smaller craters.
Part A : Craters of the group IV .
Part B : Craters of the group III .
FIG. 21
Diameter of craters in miles
Difference of the albedo from outside to the center of craters
20
16
12
8
4
0
4
8
12
16
20
24
28
-0.08
-0.06
-0.04
-0.02
0
0.02
0.04
0.06
0.08
0.10